Squeezing Atoms Using a Confinement Potential

A Thesis presented in fulfillment of the requirements for the degree of

Master of Science in Mathematical Physics

Massey University, Albany
New Zealand

Julianne Neilson Coxe
Supervisor: Peter Schwerdtfeger

2010

Abstract

Understanding the complexities of the interior of planets and stars requires the help of analyzing the effects of high pressures on certain elements believed to be found within. The Hartree-Fock method uses the Schrödinger equation, Kummer's differential equations and a confinement potential to simulate an atom being squeezed to high pressures. The Hartree-Fock method was used to calculate the total energies of atoms. After being compared to Gaussian03 and VASP, the results were deemed accurate. It was also observed that the pressure versus density data closely approximated those pairs found in outer space in the interiors of, for example, Jupiter.

Acknowledgments

To Massey University and Gaven Martin for allowing me the privilege of studying at this fine institution. ⋆ To Peter Schwerdtfeger for his vision, his help and his suggestion for me to complete a Masters degree. ⋆ To Christian Thierfelder for his patience, thorough explanations, encouragement and assistance. ⋆ To Detlev, Andreas and Matthias for their help, patience and stimulating lunch conversations. ⋆ To Elke for proofreading my thesis more than one time. ⋆ To Thomas Proffen and Tony Burrell without whom I would not be in New Zealand. ⋆ To my parents for their unending love and encouragement. ⋆ And to God for his wonderful love and mercy in giving me all of the courage, patience and perseverance I needed to complete this challenge.

Contents

List of Figures

List of Tables

1 Introduction

We had the sky up there, all speckled with stars,
and we used to lay on our backs and look up at them,
and discuss about whether they were made or only just happened.
- Mark Twain, 1835-1910, *Huckleberry Finn*

Figure 1.0.1: Supernova 1987A witnessed on Feb. 23, 1987 in the Large Magellanic Cloud, a nearby galaxy [1]. It was the closest supernova to have occurred since SN 1604, discovered by Kepler in 1604. The magnitude of brightness was so high that it could be viewed with the naked eye.

The unimaginable levels of pressure present in planets, stars and the supernova as shown above, and others like it, have inspired further research in high-pressure physics for centuries. Approximately 168,000 years ago, the core of Sanduleak $-69°$ 202, the blue supergiant star of about 18 solar masses, imploded on itself creating a shockwave that stalled as the outer layers crashed in upon the core [2]. A neutrino burst revived the shockwave which reached the surface of the star and led to the star's explosion. Detailed photographs, such as Figure 1.0.1, display the remnants of this high-pressure explosion as a cloud circled by three rings. It is believed that these rings were formed by ejections of the star's outer layers 20-thousand years before the supernova. The outstanding conjecture is the existence of a quark star instead of a neutron star in the center of the remnant [3]. The quark star would be harder to detect than a neutron star's pulses, thus explaining the lack of detection of a neutron star in the cloud.

As stars progress in years, their construction weakens and is unable to support the pressure of the outer layers as they are drawn to the core by gravity. Depending on their mass, these older stars are predicted to die in certain ways. Supergiants, like

Sanduleak -69° 202 which have 10 to 70 times the mass of our Sun, are expected to explode and coruscate, creating a supernova under the high pressure. They are believed to create so much pressure, energy and force upon becoming a supernova that the entire mass of the star is either sucked into a singularity, a black hole, or crammed into a neutron star, a dull pulsing star. Stars around one solar mass are thought to condense to become a white or brown dwarf. All options transform the high-pressure plasma and gases into a higher density, and often higher pressured, situation.

Our Sun is a younger and closer example of these high pressures found in space. High pressures vaulting into the Peta-Pascal range are believed to exist in the Sun's core descending to well below the Earth's atmospheric pressure, 101.325 kPa, in the Chromosphere. Results from theoretical calculations suggest strongly the possibility of exploring the behavior of one hydrogen atom in parallel with the known phenomena in the Sun, other stars and planets. By comparing the results to different equations of state, the reactions of hydrogen, helium and neon under such a force may be discovered.

Although much is known about the Sun, it is not so for Jupiter, figure 1.0.2 and the gas giants. Although at least 16 of Jupiter's 63 *satellites*, or moons, have been extensively analyzed down to their core [5], nothing is known, beyond theory, about the center of their gravitational orbit. This is due to the high pressure environment that exists beneath its 50 km layer of dense clouds. Space probes, like Galileo, are not able to penetrate the planet for more than an hour before losing contact with Earth [6] and telescopes, such as the Hubble, cannot pass farther than the troposphere, where temperature decreases rapidly with altitude. Jupiter is projected to be consisting of $50 - 70\%$ hydrogen [7] by mass and contain helium, neon and a range of other elements. The published estimates of the level of pressure found below 950 km into the Jovian atmosphere varies from 70 MPa [7] to 4 TPa [8] and calculated values can be found within these limits. This suggests that theoretical calculations of density

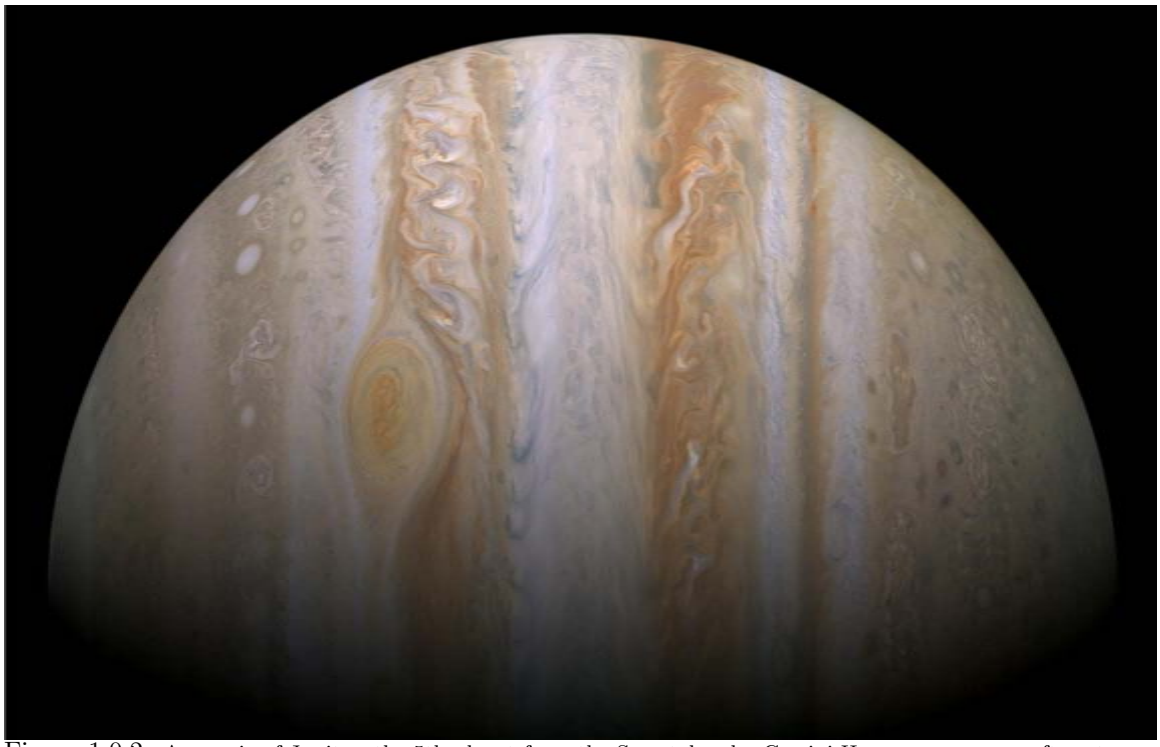

Figure 1.0.2: A mosaic of Jupiter, the 5th planet from the Sun, taken by Cassini-Huygens, a spacecraft sent on a mission to collect information on Saturn. Approximately 10 million kilometers away, Cassini passed by Jupiter upon capturing this collective image [4].

and pressure for hydrogen, helium and neon could help to clarify the picture.

A hypothetical situation, gathered from analysis of static models with the same gravitational fields, suggests that Jupiter may not have a solid core [7]. The research has shown that the hypothetical core should be anywhere between 14 Earth masses to non-existent. The lack of clarity surrounding the hydrogen-helium equation of state hinders the acquisition of a lower bound for the mass of a solid core for Jupiter.

Coming back to Earth, high pressure physics has become a popular field since the 1930's, motivated by the realization of the lack of knowledge about our universe. The extremely high pressures found inside stars and planets, like our own, have yet to be completely understood. The gravitational pull of a neutron star places pressures upon particles believed to create environments with a density 100 trillion times that of water [9]. Experimentally, only pressures up to the Tera-Pascal range have been achieved. While these are high pressures on Earth, pressures occurring throughout the galaxy span far beyond this range.

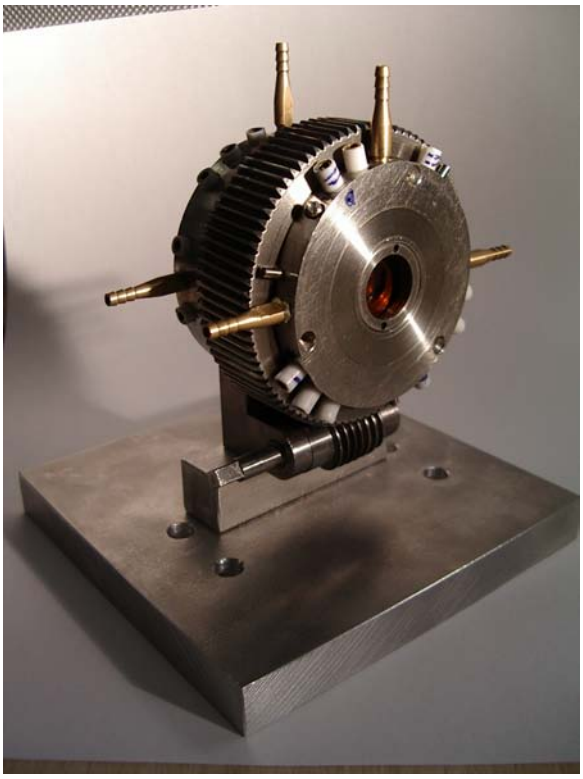

Figure 1.0.3: A diamond anvil cell often used for high pressure experiments [10].

Nevertheless, studying the effects of squeezing atoms or molecules is important as many have realized that putting bulk material under pressure can significantly change properties and chemical and physical behavior. For instance, Matsouka and Shimizu [11] have shown that the structure of bulk Lithium changes from a simple cubic lattice into a material with curiously high electrical resistance dependent on the temperature applied similar to a semi-conductor. This is quite different from the 'simple metal' status it originally acquired. In most high pressure experiments, pressures of only 200 GPa have been achieved using diamond anvils [12], like the one in Figure 1.0.3. Theoretical calculations could assist these experiments to analyze effects of pressures into the Tera-Pascal range and higher, which is currently beyond the experimental limit.

Many research topics have focused on the hydrogen atom. At extremely high pressure, it is known that it becomes metallic in nature [13], just as it is predicted to be inside Jupiter. Confining atoms, using theoretical methods, has been studied

by theoreticians for several decades and it is clear that such phenomena cannot be explained at the single-atom level. However, what happens on the atomic level while these properties are changing on a grander scale?

Looking at a model of a single hydrogen atom may lead to answers. Because of its simple nature, it is easy to understand as the model will help demonstrate what occurs at the lowest level of complexity. Modeling atoms under pressure leads to Kummer's differential equation with special boundary conditions, which is also interesting from a mathematical point of view. This thesis intends to present findings resulting from such an analysis of single-atom confinement for hydrogen, helium and neon in their stationary states. Beginning with the Schrödinger equation, the energy of each squeezed atom was calculated and used to decipher the inner workings of this high pressure environment. At the bulk-material level, there are interatomic reactions and intraatomic reactions that are taken into account as a mass is put under pressure. However, which of these reactions are more important? This thesis argues that it could be possible that the intraatomic interactions could be more important, thus, the larger-scale high-pressure system may be able to be estimated by the smallest of scales. This thesis intends to find whether or not these conditions are met.

2 Theoretical Background

2.1 The Schrödinger Equation

The Schrödinger equation for the stationary state of a many-electron system,

$$\hat{H}\Psi = E\Psi, \tag{1}$$

gives the total energy for an atom with N electrons. $\hat{H}$ is the Hamiltonian operator, Ψ is the total electronic wave function dependent on the particle coordinates $\tilde{\mathbf{r}}_\mathbf{i} = (r_i, \theta_i, \phi_i)$ and E is the total energy of the system. For an N-electron system that includes an atomic nucleus of charge Z, the Hamiltonian in atomic units is given by:

$$\hat{H} = \sum_{i=1}^{N} \left(-\frac{1}{2}\nabla_i^2 - \frac{Z}{r_i} \right) + \sum_{i>j}^{N} \frac{1}{r_{ij}}, \tag{2}$$

where r_i is the distance from the nucleus to the i^{th} electron, $-\frac{1}{2}\nabla_i^2$ is the kinetic energy of the i th electron and r_{ij} is the distance between the i^{th} and j^{th} electrons. For the single-electron problem, the Hamiltonian simplifies to:

$$\hat{H} = -\frac{1}{2}\nabla^2 - \frac{Z}{r}, \tag{3}$$

where the electron index $i = 1$ is now dropped. For a hydrogen-like atom, i.e. an atom with only one electron, an analytical solution can be found. Upon substituting (3) into (1), the equation becomes:

$$-\frac{1}{2}\nabla^2\Psi - \frac{Z}{r}\Psi = E\Psi, \tag{4}$$

in which the total wave function becomes a separable equation such that:

$$\Psi(r, \theta, \phi) = \frac{1}{r}P_{nl}(r)Y_{lm}(\theta, \phi), \tag{5}$$

where Y_{lm} are the spherical harmonics, P is the radial function, n is the principal quantum number and l is the angular quantum number. The radial function is the solution to the radial differential equation:

$$\left[-\frac{1}{2}\frac{d^2}{dr^2} - \frac{Z}{r} + \frac{l(l+1)}{2r^2} + E \right] P(nl; r) = 0, \tag{6}$$

fulfilling the boundary conditions $P(nl; 0) = 0$ and $P(nl; r) \to 0$ as $r \to \infty$ for regular solutions. The spherical harmonic equation, depending upon θ and ϕ, is

$$\Delta_{\theta,\phi}Y_{lm}(\theta, \phi) = -l(l+1)Y_{lm}(\theta, \phi), \tag{7}$$

where $\Delta_{\theta,\phi}$ is derived from the Laplace operator in polar coordinates. Since it has no

dependence on the energy value, it is sufficient to focus solely on the radial equation for this discussion.

In the next step, it is convenient to normalize these radial equations, or eigenstates, by satisfying:

$$\int_0^\infty dr P_{nl}^2(r) = 1. \tag{8}$$

This scales the values of these eigenfunctions by restricting $P_{nl}(r)$ with limiting functions that will make sure the function will act regularly at the origin and as it reaches infinity (the asymptotic limit). At the origin, the function can either resemble:

$$P(r) \to \begin{cases} r^{l+1} & \text{regular at the origin, or} \\ r^{-l} & \text{irregular at the origin.} \end{cases} \tag{9}$$

Then, as the function extends to infinity, $P(r)$ can act like either:

$$P(r) \to \begin{cases} e^{-\lambda r} & \text{regular at infinity, or} \\ e^{\lambda r} & \text{irregular at infinity.} \end{cases} \tag{10}$$

where $\lambda = \sqrt{-2E}$ [14]. Therefore, the final equation that will be regular at both the origin and near infinity becomes the following:

$$P(r) = r^{l+1} e^{-\lambda r} F(r), \tag{11}$$

where $\frac{d}{dr}F(r) \to 0$ as $r \to 0, \infty$. This will lead to the second task which is to calculate these energy eigenfunctions. By inserting equation (11) into equation (6) and simplifying, equation (6) becomes:

$$2\lambda r \frac{d^2}{dr^2}F(r) + 2\left(l + 1 - \lambda r\right)\frac{d}{dr}F(r) - \left[l + 1 - \frac{Z}{\lambda}\right]F(r) = 0. \tag{12}$$

Using a change of variables, $t = 2\lambda r$ and $k = \frac{Z}{\lambda}$, and simplifying gives:

$$t\frac{d^2}{dt^2}F(t) + (2l + 2 - t)\frac{d}{dt}F(t) - (l + 1 - k)\,F(t) = 0. \tag{13}$$

It can then be shown that the solutions to the above equation, $F(r)$, will satisfy Kummer's differential equation. This classifies each solution as a confluent hypergeometric function.

2.2 Kummer's Differential Equation

Before moving on to the application of a confinement potential, it would be most helpful to explain, a bit deeper, how the solution to the radial function is attained. It can be shown that the radial Schrödinger equation, (6), can be transformed into a special type of Kummer's differential equation. By following the calculations in the previous section, it is obvious that equation (13) is a Kummer differential equation:

$$x\frac{d^2F}{dx^2} + (b - x)\frac{dF}{dx} - aF = 0, \tag{14}$$

such that $x = t$, $b = 2l + 2$ and $a = (k - l - 1)$. This can normally be represented as a series such that:

$$F(a; b; x) = \sum_{\nu=0}^{\infty} \frac{(a)_\nu}{(b)_\nu}\frac{x^\nu}{\nu!}, \tag{15}$$

where for large x:

$$F(a, b, x) \to \frac{\Gamma(b)}{\Gamma(a)}e^x x^{a-b}\left[1 + O(|x|^{-1})\right], \text{for } x \to \infty, \tag{16}$$

where $\Gamma(z)$ is a gamma function and O is the collection of negligible terms of order $|x|^{-1}$ or less. As seen in equation (16), the solutions display asymptotic behavior for large $|x|$ values. This implies that, in order to obtain normalizable solutions, restrictions need to be placed on the coefficient of the exponential in equation (16). This is realized by forcing $\Gamma(a) = \infty$ and $\Gamma(b) \neq 0$. In using this equation for F, it

is inserted into the equation for the radial wave function, equation (11), and a final equation is quickly attained by utilizing associated Laguerre polynomials such as:

$$L_n^{(m)}(z) = \frac{(n+m)!}{n!m!} F(-n; m+1; z), \tag{17}$$

which then results in a final general wave function given by:

$$P_{nl}(r) = N_{nl} \left(\frac{2Zr}{n}\right)^{l+1} e^{-Zr/n} F\left(-n+l+1; 2l+2; \frac{2Zr}{n}\right), \tag{18}$$

where N_{nl} is a normalization constant [15].

Let us take a step back to the physics of these calculations. Each wave function, $P_{nl}(r)$, is correct mathematically, but not all of them apply physically. The ones that do apply have specific qualities in common. These functions apply to those where $a = n_r$, where n_r is the number of nodes of the radial wave function, and $\Gamma(b) \neq 0$. These two qualities assure a normalizable solution will be the outcome. Furthermore, when expressed in this form, $a = l+1-Z/\lambda$, the energy eigenvalues can be extracted from the obvious relationships between λ and the energy, E, where $\lambda = \sqrt{-2E}$. This relation gives the equation to calculate the energy eigenvalues,

$$E_n = \frac{-\lambda_n^2}{2} = -\frac{Z^2}{2n^2}, \tag{19}$$

where each E_n has n radial wave functions which are the aforementioned $P_{nl}(r)$ solutions. Thus, the lowest eigenstates of a hydrogen atom have the following radial wave functions, $P_{nl}(r)$:

$$
\begin{aligned}
P_{10}(r) &= 2Z^{3/2} r e^{-Zr}, \\
P_{20}(r) &= \frac{1}{\sqrt{2}} Z^{3/2} r e^{-Zr/2} \left(1 - \frac{1}{2} Zr\right), \\
P_{21}(r) &= \frac{1}{2\sqrt{6}} Z^{5/2} r^2 e^{-Zr/2}, \\
P_{30}(r) &= \frac{2}{3\sqrt{3}} Z^{3/2} r e^{-Zr/3} \left(1 - \frac{2}{3} Zr + \frac{2}{27} Z^2 r^2\right), \\
P_{31}(r) &= \frac{8}{27\sqrt{6}} Z^{5/2} r^2 e^{-Zr/3} \left(1 - \frac{1}{6} Zr\right), \\
P_{32}(r) &= \frac{4}{81\sqrt{30}} Z^{7/2} r^3 e^{-Zr/3}.
\end{aligned}
$$

which are plotted in Figure 2.2.1.

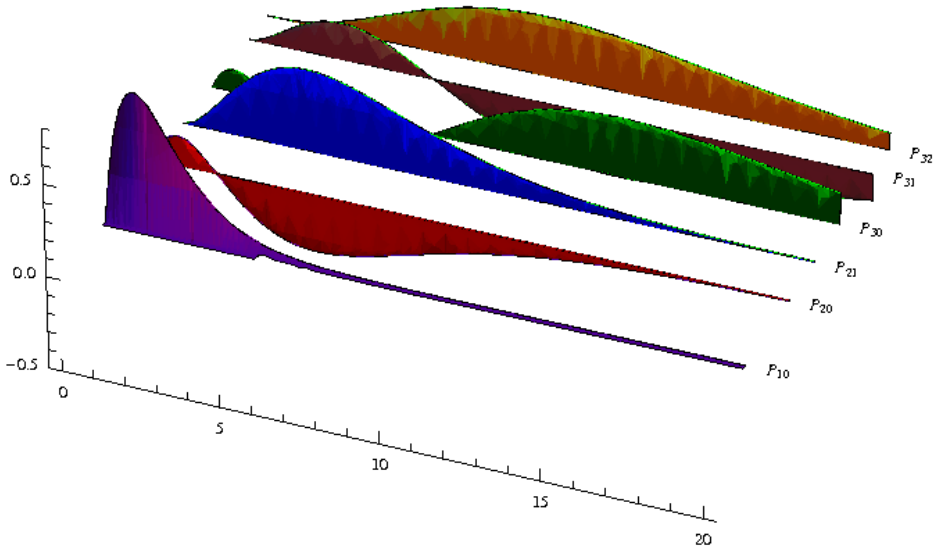

Figure 2.2.1: Normalized Coulomb potential wave functions for hydrogen plotted against the radius [16].

2.3 Multi-Configuration Hartree-Fock

The computer program utilized in this thesis uses the Multi-Configuration Hartree-Fock approximation to calculate the energies of atoms. This section gives a brief overview of the theory used in the program.

The purpose of the Hartree-Fock method is to *retain the simplicity of the independent single-particle picture and to approximate an exact solution on the N-electron problem as well as possible within this framework* [17]. The method begins by finding a Slater determinant, which by definition is a determinant consisting of all of the products of the wave functions, given by:

$$\Psi = \begin{vmatrix} \psi_1(x_1) & \psi_1(x_2) & \cdots & \psi_1(x_N) \\ \vdots & \vdots & & \vdots \\ \psi_N(x_1) & \psi_N(x_2) & \cdots & \psi_N(x_N) \end{vmatrix}, \tag{20}$$

where x_i is the collection of spatial and spin coordinates for each electron, i. It is mandatory that the Slater Determinant satisfies the Pauli Principle which states that no two fermions [electrons] can occupy the same single-particle state. This is easily attained since any Slater Determinant, by definition, is antisymmetric which is equivalent to the Pauli Principle requirement regarding fermions. This basically means that if the order of two or more single particle functions are changed, the determinant is multiplied by -1 for every pair that is changed.

Using a Thomas-Fermi initial guess, the best Slater determinant is found using a self-consistent method. This best determinant will fulfill the requirements of Brillouin's theorem: all matrix elements of $\hat{H}$ [the Hamiltonian] between Ψ and one-particle-one-hole extensions vanish such that:

$$\delta E[\Psi] = 0 \Longleftrightarrow \langle \Psi_{\alpha\beta} \mid \hat{H} \mid \Psi \rangle = 0, \forall\ \Psi_{\alpha\beta}, \tag{21}$$

where α and β are unoccupied and occupied single-particle states and

$$\delta E = E[\psi + \delta\psi] - E[\psi]$$

which vanishes if and only if $\langle\delta\psi|\hat{H} - E|\psi\rangle + \langle\psi|\hat{H} - E|\delta\psi\rangle$. Solving this results in a set of equations known as the Hartree-Fock equations [17]:

$$\begin{aligned}\langle\psi_\alpha \mid \frac{\hat{\mathbf{p}}^{\mathbf{2}}}{2\mu} + \hat{V} \mid \psi_\beta\rangle + \sum_{i=1}^{N}\Big(\langle\psi_i\psi_\alpha \mid \hat{W} \mid \psi_i\psi_\beta\rangle - \langle\psi_i\psi_\alpha \mid \hat{W} \mid \psi_\beta\psi_i\rangle\Big) \\ = \langle\psi_\alpha \mid \hat{h}_\psi \mid \psi_\beta\rangle = \epsilon_\alpha\delta_{\alpha,\beta}\end{aligned} \tag{22}$$

where, again, ψ_α and ψ_β are any unoccupied and occupied single-particle states, respectively, while the sum only runs over single-particle states occupied in Ψ. This equation corresponds to the one-body Hamiltonian:

$$\hat{h}_\Psi = \frac{\hat{\mathbf{p}}^{\mathbf{2}}}{2\mu} + \hat{V} + \hat{W}_d - \hat{W}_{ex}, \tag{23}$$

where $\frac{\hat{\mathbf{p}}^{\mathbf{2}}}{2\mu}$ is the kinetic energy, μ is the reduced mass, $\hat{V}$ is the one-body potential, $\hat{W}_d$ is the local potential and $\hat{W}_{ex}$ is the exchange potential. The first two terms originate from the N-body Hamiltonian and do not depend on the Slater determinant and the second two are one-body operators defined by their matrix elements.

The Hartree-Fock approximation uses a mean-field approximation that estimates the effective potential part, $\hat{W}_{ex}$, of the Hamiltonian to be of the form:

$$V_{eff}^n = -\frac{Z}{r} + \int \frac{\rho(r')}{|r - r'|}d^3r', \tag{24}$$

where $\rho(r') = \tilde{\Psi}^*(r')\tilde{\Psi}(r')$. This condenses all other wave functions into one making the problem easier to solve. The Schrödinger equation then resembles:

$$-\frac{1}{2}\Delta\Psi^n + V_{eff}^n\Psi^n = E^n\Psi^n, \tag{25}$$

for a 1-particle function with electron, n. By applying slight adjustments, each wave

function gradually approaches a limit. These adjustments follow the *self-consistent method* of:

- Determine Slater determinant, Ψ_0,
- Diagonalize one-body Hamiltonian, $\hat{h}_\Psi$,
- Obtain new single-particle states,
- Find a new Slater determinant, Ψ_1,
- Repeat.

The final Hartree-Fock energy, $E[\Psi_{HF}]$, will not be the same as the summation of the single-particle energies of the occupied states, ϵ_i, because the latter will double count part of the exchange energy between electrons. The Hartree-Fock energies are procured from the combination of the equation for the orthonormal single-particle states and the two-body operators which gives:

$$\begin{aligned}\langle \Psi_{HF} \mid \hat{H} \mid \Psi_{HF} \rangle &= \sum_{i=1}^{N} \langle \psi_i \mid \frac{\hat{\mathbf{p}}^{\mathbf{2}}}{2\mu} + \hat{V} \mid \psi_i \rangle \\ &\quad + \frac{1}{2} \sum_{i,j=1}^{N} \Big(\langle \psi_i \psi_j \mid \hat{W} \mid \psi_i \psi_j \rangle - \langle \psi_i \psi_j \mid \hat{W} \mid \psi_j \psi_i \rangle \Big) \\ &= \sum_{i=1}^{N} \epsilon_i - \frac{1}{2} \sum_{i,j=1}^{N} \Big(\langle \psi_i \psi_j \mid \hat{W} \mid \psi_i \psi_j \rangle - \langle \psi_i \psi_j \mid \hat{W} \mid \psi_j \psi_i \rangle \Big) .\end{aligned} \tag{26}$$

To properly solve for the total energy, the sum of multiple Slater determinants is used. This works quite well for lighter elements whose relativistic corrections are easily treated with first-order perturbation theory. However, for heavier element energies, the use of a Dirac equation can be a helpful replacement for the Schrödinger equations, where the numerical calculations can become impossible.

The Multi-Configuration Hartree-Fock approximation goes one step further by calculating the final wave function as a linear combination of a number of other

strategically calculated wave functions. These functions represent each of the different configurations of the atom's electrons in the occupied orbitals and the virtual orbitals. The resulting linear combination is then used as the radial wave function and the energy is calculated.

This thesis only manipulated the local potential but did not change any other part of the program.

2.4 Analysis of Data

After the energy calculations were made, the evaluation of the data began. The volume, V, pressure, P, and density, ρ:

$$V = \frac{4}{3}\pi r_o^3, \tag{27}$$

$$P = -\frac{1}{4\pi r_o^2}\frac{dE}{dr}\Big|_{r_o}, \tag{28}$$

$$\rho = \frac{m}{V}, \tag{29}$$

respectively, were calculated and investigated as functions of n and r_o, where r_o is the confining radius and n is the power of the stiffness potential.

These expressions are easily obtained from the correct definition for the pressure of a system:

$$P = -\frac{dE}{dV}, \tag{30}$$

$$= -\frac{dE}{dr}\frac{dr}{dV}. \tag{31}$$

Now it is obvious that by solving the volume equation for r, finding $\frac{dr}{dV}$ is easily completed. By evaluating:

$$\frac{dV}{dr}\Big|_{r_o} = \frac{d}{dr}\left(\frac{4}{3}\pi r^3\right)\Big|_{r_o} = 4\pi r_o^2 \tag{32}$$

which then gives an equation that can be simplified:

$$\frac{dr}{dV}\Big|_{r_o} = \frac{1}{\frac{dV}{dr}}\Big|_{r_o} = \frac{1}{4\pi r_o^2} \tag{33}$$

This is replaced into equation (31) which results in:

$$P = -\frac{1}{4\pi r_o^2}\frac{dE}{dr}\Big|_{r_o}, \tag{34}$$

where $\frac{dE}{dr}$ is calculated numerically using the definition of derivative to supply the final pressure equation given previously in equation (28).

The pressure versus density plots, in particular, are important to this work because the data will be able to be compared to experimental pressures. Moreover, they can be compared to the pressures and corresponding densities predicted for the Sun and other larger stars.

Next, according to the Thomas-Fermi theory, the Particle-in-a-Box law the pressure can be related to the volume in such a way that the latter can be calculated from the former using this relation:

$$V = bP^{-3/5}, \tag{35}$$

where b is a constant factor. Using this equation will check whether or not our calculations of pressure and energy are in the right order of magnitude. This deviates from the Ideal-Gas law:

$$V = cP^{-1}, \tag{36}$$

where c is a constant.

3 Computational Details

3.1 MCHF95

In order to study atoms under pressure, the computer program MCHF95 [18], Multi-Configuration Hartree-Fock, was applied. It is a FORTRAN 77 program that uses the Hartree-Fock approximation to calculate the total electronic energy of an atom. It uses the Schrödinger equation for the steady-state of a many-electron system [19].

In MCHF95, Numerov's method is used to calculate the solutions to the Coulomb wave function [20]. To use this method, the equations must be of the form:

$$\left[\frac{d^2}{dx^2} + F(r,l)\right] u(r) = 0. \tag{37}$$

To solve this equation, MCHF employs the three-point method with the recursive relation:

$$w_{r+h} = \left(2 + h^2 F(r,l)\left(\frac{1}{1 - \frac{h^2}{12}F(r,l)}\right)\right) w_r - w_{r-h}, \tag{38}$$

where

$$F(r,l) = V(r) + \frac{l(l+1)}{2r^2} - E. \tag{39}$$

The rest of the refinement of the radial function is a combination of normalization techniques, checking for orthogonalization and adjusting the constants such that the wave function is more accurate.

The confinement potential is easily added as a local potential directly in the input file. Upon defining the Hamiltonian, equation (2), the confining potential is added to simulate the squeezing of an atom. The confinement potential chosen here is of the form,

$$V(r) = \left(\frac{r}{r_o}\right)^n, \tag{40}$$

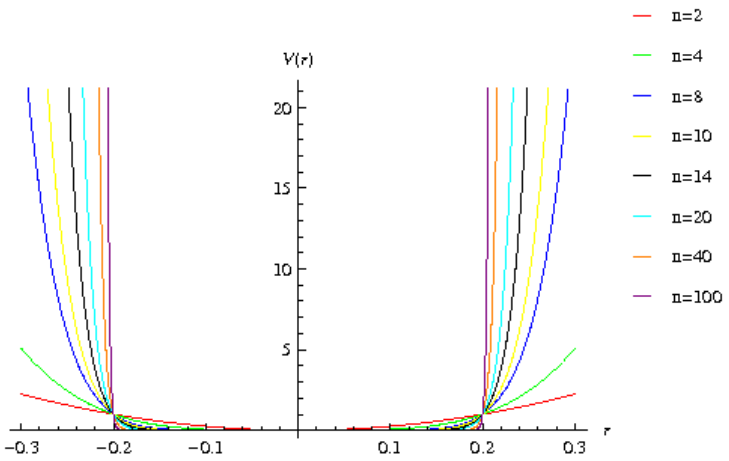

Figure 3.1.1: Examples of the confinement potential when $r_o = 0.2$ and the stiffness, $n \in [2, 100]$.

where r is the distance between the nucleus and the electrons. The effects of this potential are seen in Figure 3.1.1. The limiting function of the equation is the hard-wall spherical potential. For $r_o \to \infty$, the limiting situation of a free atom is obtained. For the case of a hard-wall confinement potential, the wave function will be forced to zero at r_o,

$$V_{HW} = \lim_{n\to\infty} \left(\frac{r}{r_o}\right)^n. \tag{41}$$

Since n can be manipulated, as well as r_o, the hardness of the potential can be varied.

3.2 Gaussian

Gaussian03 [21] is a quantum chemical suite, but with a few differences compared to MCHF95. Although Gaussian03 does use the Hartree-Fock method, it uses Gaussian functions to expand the exact wave function instead of the numerical Hartree-Fock method of MCHF95. As the procedure to solve Gaussian functions is much more elaborate than the numerical one, it takes much longer in computer time to obtain the electronic energies. However, MCHF95 not only takes just a few seconds for a small atom, but the results are much closer to the exact eigenvalues for the hydrogen atom. Another difference is that Gaussian can calculate the energies for a more complex

many-particle system such as a molecule, not just one atom like in MCHF95. Gaussian is used in place of MCHF95 when the numerical calculations become impossible, which occurs when properties are calculated or when electron correlation is taken into account.

Data representing the same confinement situations from MCHF95 were compared to the newly calculated energies of Gaussian03. The basis set used was user-defined and specific confinement potentials were applied in the input file. Most combinations of potentials and confinements were calculated without any problems. However, the integral code in Gaussian could not handle the ranges of radii or potential values used for MCHF95 calculations. This may be because the way in which it was manipulated is not the program's primary function. Therefore, it was not applicable for a stiffness of $n > 14$ in the confinement potential for all three elements and for $r_o < 1.3$ a.u. for Neon.

3.3 VASP

The final program used to compare the MCHF95 values was the Vienna *Ab initio* Simulation Package, VASP [22]. This package uses density functional theory (DFT) to calculate ground-state properties of crystalline solids, like the solid hydrogen calculated in this work. In order to properly model the electron-electron interactions and the exchange-correlation energy, the generalized gradient approximation (GGA) by Perdew, Burke and Ernzerhof [23] was used. The interactions between the electrons were modeled using the projector augmented wave method (PAW) [24, 25] which allows the expansion of the electronic wave functions to be restricted to a cut-off energy of 1000 eV but still gives access to the all-electron wave functions in the atomic core regions as well. Brillouin zone (BZ) calculations used a regular mesh in reciprocal space and 512 $\mathbf{k}$ points in the BZ of atomic hydrogen. The cell lattice vectors and internal coordinates for a certain number of given cell volumes were optimized in order to find the minimal energy structure within DFT-GGA. This was done by using

a conjugate-gradient or quasi-Newton algorithm to minimize the Hellmann-Feynman forces. The structure is then in equilibrium if each Cartesian component of the atomic forces is below 5 meV/Å. The derivative, $\frac{dE(V)}{dV}$, was then analytically calculated from the data to compare to the MCHF95 pressure values.

4 Results: Hydrogen, Helium and Neon

4.1 Hydrogen

Since the spectrum of the hydrogen atom for a point nucleus can be obtained analytically, this system provides a stringent test for every numerical treatment. In the following, the squeezing of a single hydrogen atom in a (im)penetrable spherical box was studied by calculating the ground state energies of this atom for different box sizes using the program package MCHF95. By varying r_o and n in the equation for the local potential, the amount of squeezing of the atom was able to be changed between the extreme cases of applying a hard-wall potential and dealing with the free unsqueezed atom. As discussed before, for $n \to \infty$ the spherical box becomes impenetrable.

4.1.1 Results and Discussion

Firstly, the effects of decreasing the softness of the potential wall were explored by increasing the exponent, n, of the confining potential of equation (40). Therefore, the ground state energies were calculated when changing n between $n = 1$ and $n \approx 100$ continuously in step sizes of 2. Due to convergence and numerical problems of the wave functions calculated in MCHF95, higher values than $n = 102$ could not be obtained in this calculation. The confining radius, r_o, was fixed at 1 atomic unit (a.u.).

Secondly, the effects of changes in the confining radius, r_o, by varying r_o between 0.2 a.u. and 10 a.u. was investigated. The hardness parameter, n, was chosen to be

30 corresponding to a relatively stiff confining potential. It was the highest value for n where no convergence problems in the whole range of radii were observed. The resulting values for the ground state energy are documented in Table 2 and the trends can most easily be seen in Figure 4.1.3.

The results from varying r_o are shown in Table 1 (see Appendix) and plotted in Figure 4.1.1. The energies are increasing with n and are very slowly approaching the limit of 2.43 a.u., the energy of a hydrogen atom confined by a hard-wall potential at $r_o = 1$ a.u. [26]. If the atoms are squeezed less, i.e. r_o is increased, the results converge much faster to the hard-wall limit, as can be seen in Figure 4.1.2. Here r_o is changed while n is set to 30. From about $r_o = 3.0$ a.u. the energies are already converged to the hard-wall values for $n = 30$. Note that for $n = 0$ we have $V(r) = 1$ and the total energy for hydrogen is shifted from -0.5 a.u. to +0.5 a.u.

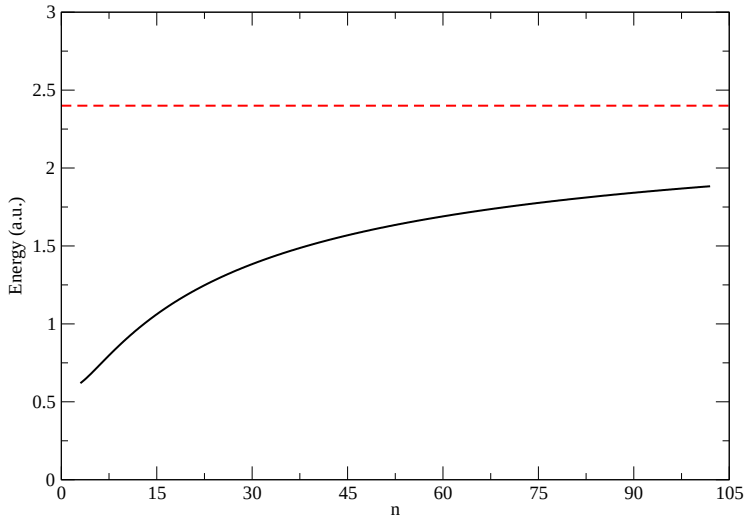

Figure 4.1.1: The ground state energy of a hydrogen atom is plotted for decreasing softness of the confining potential (the solid line), realized by increasing the potential parameter n. As n tends towards infinity, the energy, E, seems like it is very slowly approaching the expected limit of 2.43 a.u. [26], the dashed line, which is the energy of a hydrogen atom confined by a hard-wall at $r_o = 1$.

The results from fixing at $n = 30$ show that, as the radius of confinement is increased, the energy values decrease monotonically to approach the energy of a free hydrogen atom as expected, which is exactly -0.5 a.u. The energy becomes negative

at about $r_o = 1.65$ a.u. for this confinement potential (see also Figure 4.1.2). This implies that when $r_o < 1.65$ a.u., the ground-state system is not bounded compared to the free atom, i.e. the system would lose an electron without being confined (or suddenly released).

In addition to studying the trends in the ground state energy when varying the confinement potential, it is also of interest to analyze the wave functions. Figure 4.1.4 shows the probability distribution functions for different confinements, from $r_o = 0.2$ to the free atom, setting $n = 30$. As r_o increases, the wave functions are less and less restricted and follow an exponential decay in the asymptotic limit.

The obvious next step was to compare the pressure, P, to the density, ρ, for the studied range of squeezing. The pressure and density are given by:

$$P = -\frac{1}{4\pi r_o^2}\left[\frac{dE}{dr}\right]_{r=r_o} \tag{42}$$

$$\text{and } \rho = \frac{3m_H}{4\pi r_o^3}, \tag{43}$$

where the mass of hydrogen, m_H, is set to 1 a.u. and the change of the energy with the radius, $\frac{dE}{dr}$, was calculated numerically from the $E(r)$ curve represented in Figure 4.1.2. Results are shown in Figure 4.1.5 which have been calculated from our data collected for r_o values in the interval of $[1.2, 10.0]$ a.u. with $n = 30$. The density is increasing with the pressure while the confinement radius is decreasing, as expected. The density values at large r_o were quite small and grew logarithmically leading to a steep increase at large r_o. This is in accordance with the well-known fact that the density increases as the pressure of a substance rises.

Results obtained by MCHF95 were cross-checked by comparing them to those obtained from using Mathematica®, see Tables 1 and 3, which allows to calculate ground-state energies within the hard-wall limit in dependence of the confinement radius, r_o [16]. The Mathematica® results were further checked by comparing the

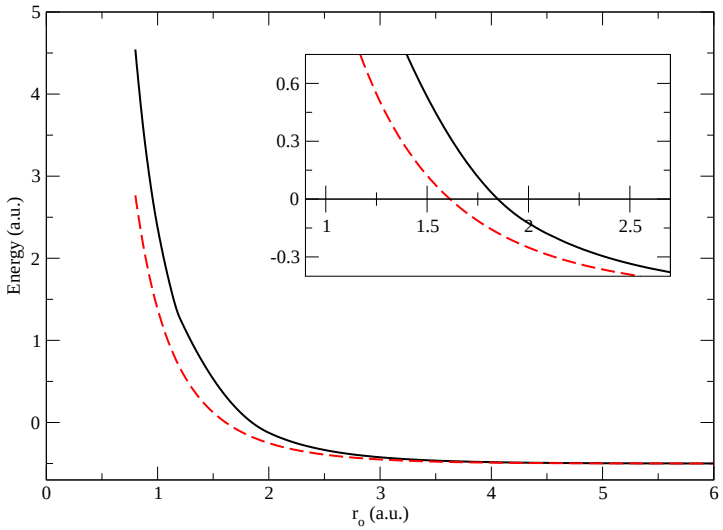

Figure 4.1.2: The ground state energy values of a hydrogen atom using a hard-wall (solid line) or confinement potential (dashed line), with $n = 30$, plotted against the corresponding radius of confinement, r_o. The inlaid graph shows the region at which the energies become negative.

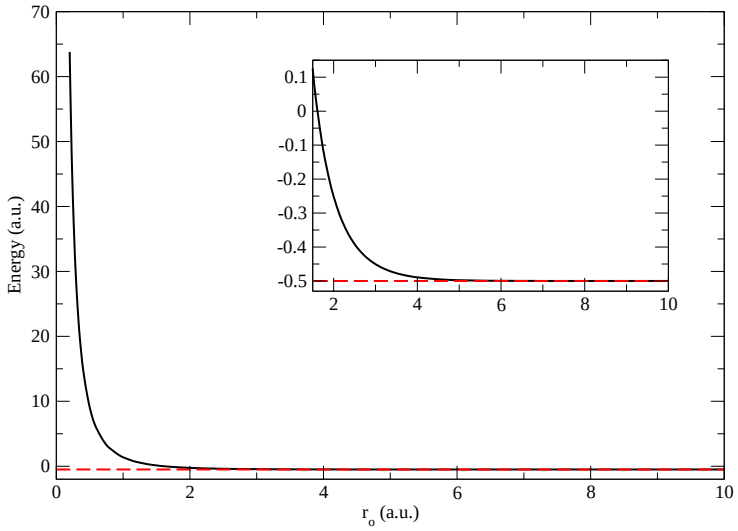

Figure 4.1.3: The ground state energy of a hydrogen atom is plotted as the confining radius, r_o, increases. As r_o increases, the energy asymptotically reaches -0.5 a.u., the energy of a free hydrogen atom shown by the dashed line. The hardness of the potential wall is set to $n = 30$. The inlaid graph shows that the values do approach -0.5 a.u.

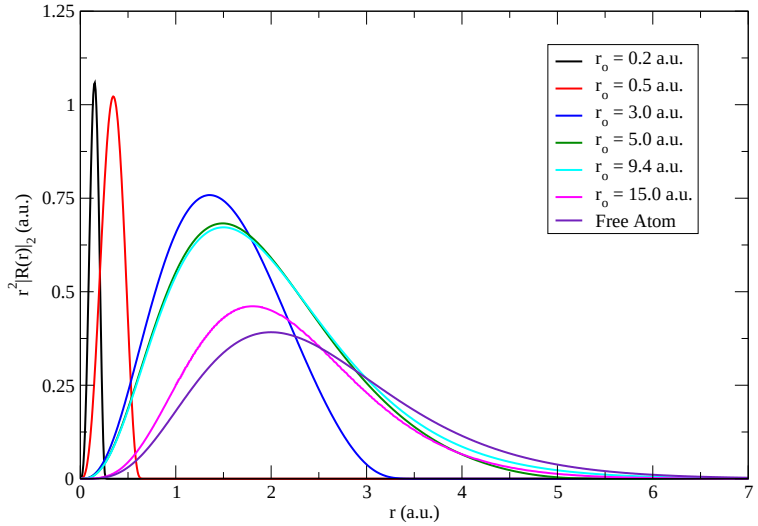

Figure 4.1.4: The probability density function of the radial distribution function, $P(r)$, at different r_o values of the confinement potential of equation (40). The parameter n is set to 30.

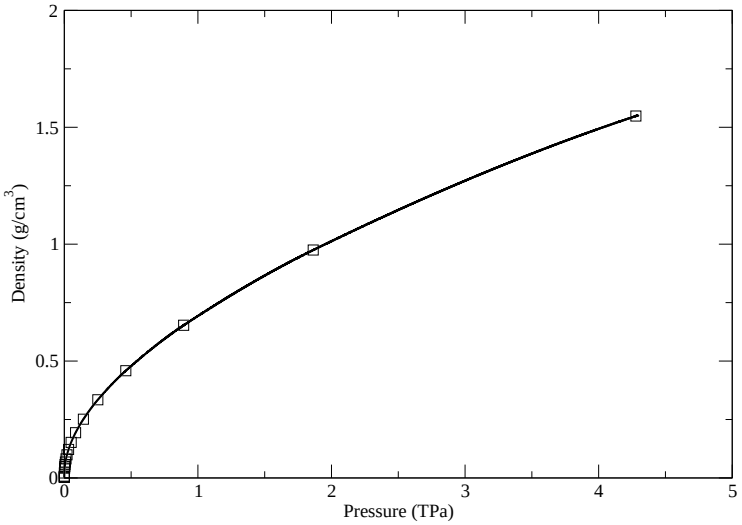

Figure 4.1.5: Pressure, P, versus Density, ρ, calculated for different confinement radii, r_o.

results for the energies of hydrogen by Ludeña [26]. They also used a hard-wall to confine hydrogen, employing a cut-off function in the context of the Roothaan-Bagus formalism. The two sets of values were the same, apart from negligible numerical noise. Then, the MCHF values were checked by comparing the energy, in Figure 4.1.2,

as well as the density and pressure values of the hard-wall confinement to those confined by potential (40). The hard-wall pressure values are plotted in Figure 4.1.6 with particles being confined to a sphere of changing radius with a confining potential of $n = 2, n = 20,$ and $n = 30$. As before, the rate of change of the pressures increased for smaller pressures/densities, i.e. large confinement radii, r_o. The experimental range of pressures does not extend to extremely high pressures; Figure 4.1.6 focuses on the experimental range equal to and below 1 TPa. However, the total range of the data extended all the way to 3.783×10^{16} Pa when the hydrogen was squeezed to a radius of 0.4 a.u.

In order to explore another way to confine an atom, the integration was performed only up to the confining radius, r_o, for the free hydrogen atom assuming that the SCF procedure takes care of the right boundary condition. The resulting energies were compared to the hard-wall and the original MCHF95 data obtained above. The results are shown in Figure 4.1.7. For $r_o \geq 4$ a.u. the obtained energies approximated the hard-wall and original energy values well, while for smaller confinement radii the deviations are quite pronounced. This can be easily understood when looking at the probability distribution shown in Figure 4.1.4. For small r_o, the tail of the wave functions lying outside the box of width r_o is much more pronounced than for large r_o, where the tails become more and more negligible. In the same manner, the energy contributions originating from these tails become smaller while increasing r_o. However, this should be remodeled in the SCF procedure. Obviously, the logarithmic grid is not sufficient to achieve high accuracy because of the lack of points in crucial areas of the wave functions. The logarithmic grid clusters more points at the beginning of the calculation and less as the radius gets larger. It is most important to have as many points as possible around the specific confinement radius that is being calculated. This interval is where the wave function goes to zero and the more points that are in that area, the more accurate the calculations will be.

Another comparison to try to describe the relation of the values that have been

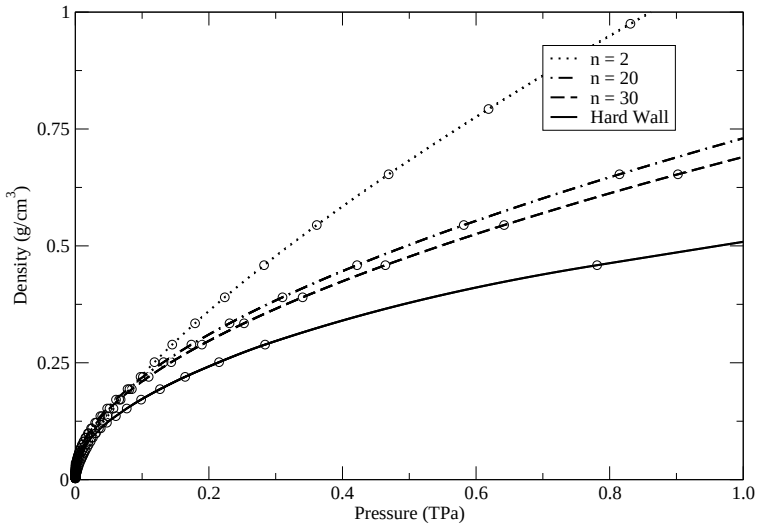

Figure 4.1.6: Values in the Tera-Pascal range of the pressure versus density values. Both the hard-wall method (solid line) and the MCHF95 method for $n = 2, 20, 30$ are represented. As to be expected, the results obtained with the confinement potential approach the hard-wall limit with increasing hardness of the potential, n.

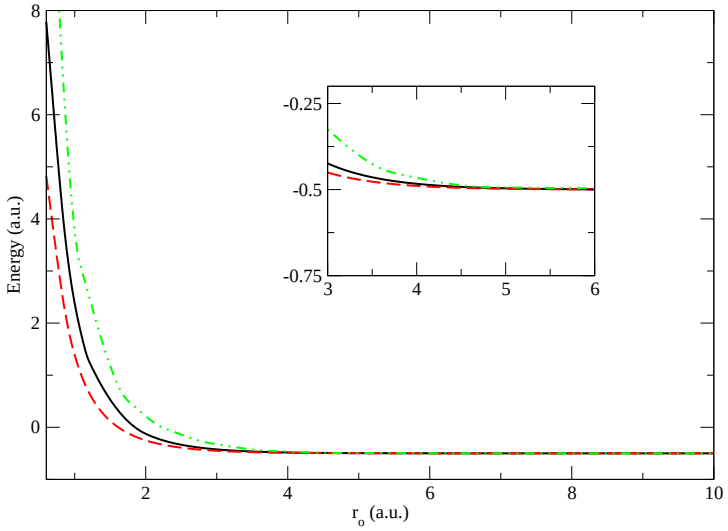

Figure 4.1.7: The energies produced by a hard-wall confinement potential (solid black line) and the original MCHF95 hydrogen energy values (dashed red line) are compared to energy values obtained by integrating the MCHF95 energy integrals only up to the confinement radius r_o (dashed green line). The hardness of the potential wall is set to $n = 30$, as before.

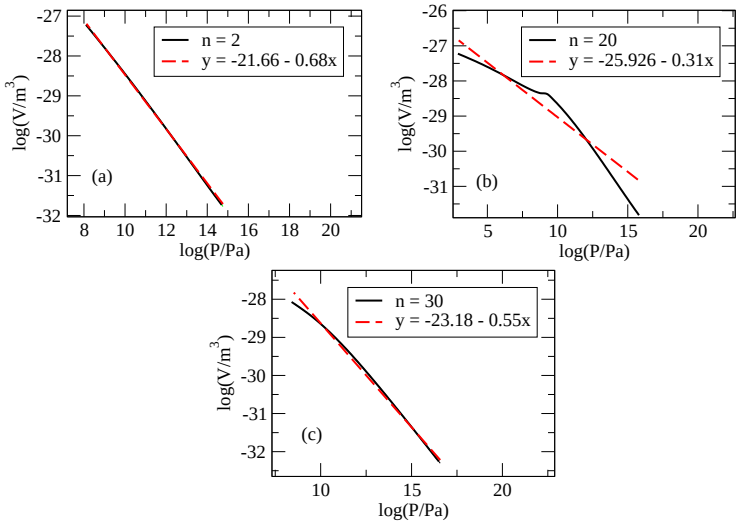

Figure 4.1.8: The log base 10 was taken of each group of pressure and volume values to compare them and decide whether or not they have a linear correspondence. Then the slopes of each linear regression were compared to the Thomas Fermi Theory or the Particle-in-a-box Law, equation (35), and the Ideal Gas law, equation (36). (a) Pressure and Volume comparison for $n = 2$ a.u. (b) Pressure and Volume comparison for $n = 20$ a.u. (c) Pressure and Volume comparison for $n = 30$ a.u.

calculated can be found in applying different relations such as the Thomas Fermi Theory, the Particle-in-a-Box Law and the Ideal Gas Law. Each compares volume to pressure using different exponents of a power law (see equations (35) and (36))). To most easily decide if any of these equations relate the pressure and volume values of these confinements, the logarithmic value for volume and pressure were calculated and a linear regression was fit to each resulting plot. These linear regressions would then correspond to a power regression for the original values. The slope of the linear equation would be the exponent for a power regression of the form

$$V = cP^{-m} \tag{44}$$

where c is a constant and $-m$ would be the slope value. The results can be seen in Figure 4.1.8. The ideal situation would result in a perfectly linear correlation between the logarithmic volume and logarithmic pressure. However, according to the figure, the higher stiffness parameters resulted in plots that are more curved than the $n = 2$ plot. This is the first clue that suggest that no such linear relation exists between these values, except for small stiffness parameters. Here, it is clear that the $n = 20$ and the $n = 30$ plots are not quite linear, rendering the former relation nonexistent and the latter relation questionable. The second suggestion is found in the slope of the regression equation. These slope values correspond to the exponents of the original power laws. Two of the slopes, $n = 2$ and $n = 30$, are quite close to the required values (-1, -0.6), but each of them deviates from one of the expected values by at least 0.05. Therefore, an acceptable deviation must be chosen in order to deem these relations applicable. Therefore, the pressure and volume values calculated cannot be described by these power laws unless an error of 0.05 can be allowed. This is not surprising since, especially for the Ideal Gas law, the relation pertains to a distribution of particles rather than a single atom. It gives an example of a situation where the bulk media may not be described by the single particle.

Next, in order to see how the theoretical gas data compared to the squeezing of

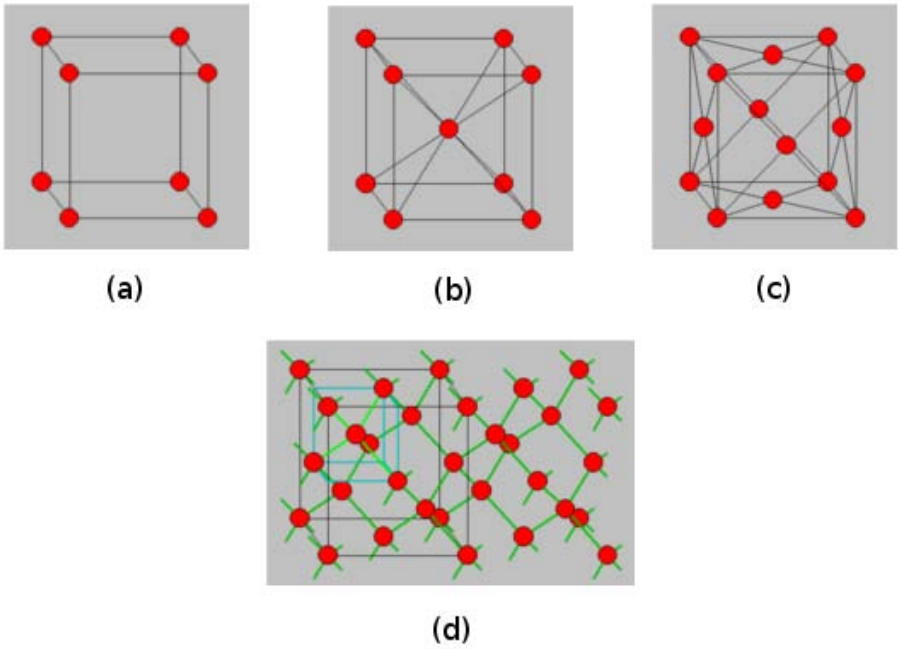

Figure 4.1.9: (a) simple cubic (sc), (b) body-centered cubic (bcc), (c) face-centered cubic (fcc), (d) diamond lattice [27].

solid hydrogen, the program package VASP [22] was used to calculate the pressure and density values for solid hydrogen. With this program, the pressure versus density curves for a variety of different hydrogen crystal structures such as simple cubic (sc), face-centered cubic (fcc), body-centered cubic (bcc) and diamond structures as shown in Figure 4.1.9 can be calculated. The pressures of the solid and the confined atom are compared in Figure 4.1.10. The pressure curves for the solid are clustered together while the single-atom pressure data are coming together as the stiffness, n, is increased. Figure 4.1.10 shows that the hard-wall potential is not a good approximation of a real physical system; nevertheless, it is fascinating that the single-atom results qualitatively reflect the trends of the confined-solid pressures as the former neglects all atomic overlaps which are present in the latter. These overlaps should lead to a binding contribution for lower pressures and thus shift the volumes of the solid to smaller values. This is indeed the case as can be clearly seen in this figure. For higher pressures, finally, the overlaps result in a repulsive interaction with the contrary effect of a volume increase which explains why the solid and atom data are

coming closer together and may even cross at extremely high pressures.

Additionally, the accuracy of our MCHF95 results for the ground-state energies were used to test the energies computed using the Gaussian03 program package [21]. Figure 4.1.11 shows perfect alignment but differences are clearly seen in Figure 4.1.12. Ultimately, the values should be the same but inefficient basis sets used in Gaussian03 cause the deviations in Figure 4.1.12. An even-tempered basis set was used by expanding scaling factors of the exponents of the Gaussian functions. However, it is obvious that an even larger expansion is required to procure a longer range of accurate results. For certain ranges of n the two data sets corresponded well. In the first figure, the calculated energies are plotted against the radius of confinement as r_o is changed. The values are identical. In the second figure, the calculated energies are plotted against the corresponding n values, while r_o was kept at 1 a.u. In this plot, one can clearly see that the Gaussian03 values deviate for values of $n > 9$. Adjustments to the basis set would fix that problem.

Finally, a comparison of calculated and previously published results for the pressure

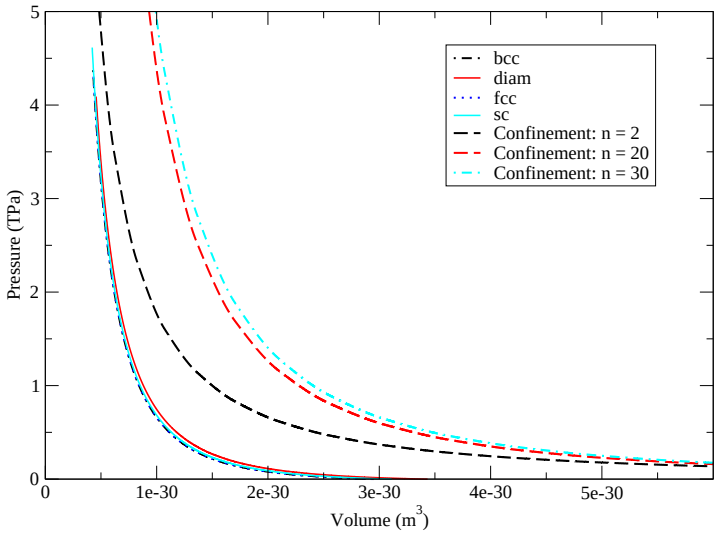

Figure 4.1.10: Volume versus Pressure plots for solid hydrogen for the different crystal structures of Figure 4.1.9, and the single-atom being confined by potentials with varying stiffness of $n = 2, 20$ and 30.

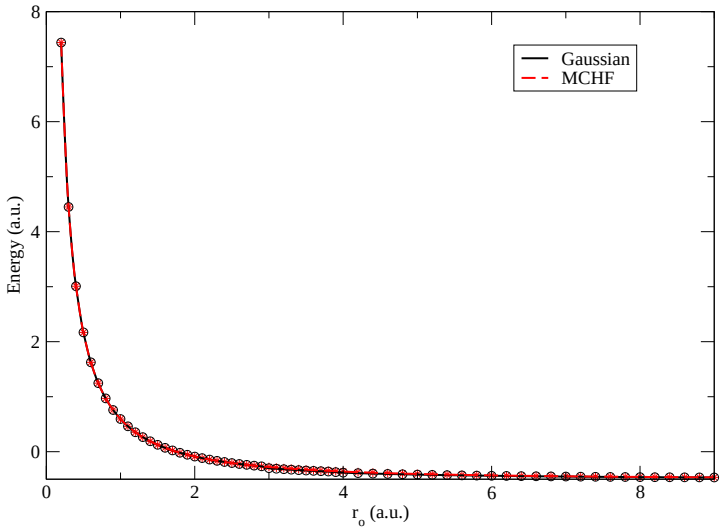

Figure 4.1.11: Energy versus the confinement radius, r_o, calculated by Gaussian and MCHF. The stiffness parameter of the potential, n, was set to 2.

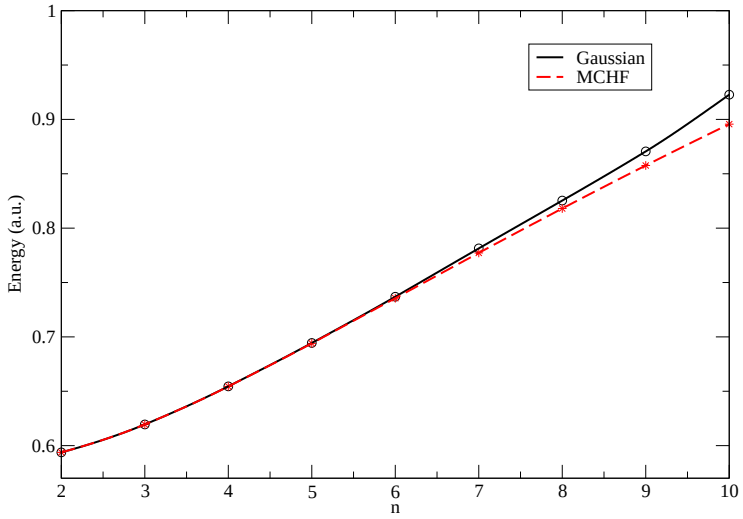

Figure 4.1.12: The stiffness potential, n, versus Energy calculated by Gaussian and MCHF, where $r_o = 1$ a.u. Data collected for $n > 10$ gave errors in the integral evaluation with Gaussian.

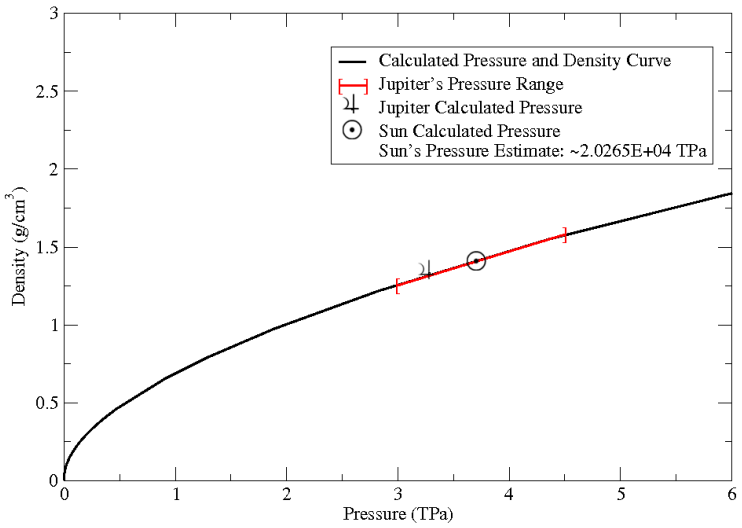

Figure 4.1.13: Expected range of values for the pressure inside Jupiter [8] and the calculated values for the Sun and Jupiter are plotted with the MCHF95 Pressure values (when $n = 30$) against the corresponding density values. The MCHF95 pressure of Jupiter and the Sun was calculated from their average densities. The Sun's expected pressure [5] is given in the legend.

and density of the Sun and Jupiter is shown in Figure 4.1.13. For the Sun, the predicted average density is $\rho = 1.408 \frac{\text{g}}{\text{cm}^3}$ [28]. Using our data computed with MCHF95, this corresponds to a pressure value of 3.6975 TPa which differs from the published maximum pressure in the Sun, $P = 2.0265 \times 10^4$ TPa [5] by 4 orders of magnitude. This clearly is attributable to temperature effects since our values are 0 K values and cannot reproduce hot plasmas.

Jupiter is projected to consist of 50-70 % hydrogen [7] at much lower temperatures, thus, our pressure calculations should be closer to other predicted values. The average density of Jupiter is $\rho = 1.33 \frac{\text{g}}{\text{cm}^3}$ [8], which corresponds to a confinement radius of $r_o = 1.26231$ a.u. For these confinement requirements and a stiff potential with $n = 30$, a pressure 3.38393 TPa for hydrogen was obtained. This falls in the calculated pressure range of Jupiter published by Elkins-Tanton [8] as seen in Figure 4.1.13.

From our studies presented here, it was concluded that using a confinement potential in order to study the squeezing of an atom promises to be a good procedure to discuss qualitative trends. Therefore, the study was expanded to elements with a larger number of particles such as Helium and Neon.

4.2 Helium

Helium, from the Greek word *Helios* for the Sun, was discovered when a new line was detected in the solar spectrum during a solar eclipse in 1868. As it contains two electrons, its energy cannot be obtained analytically, in contrast to hydrogen. It is also a closed-shell element. It is in the group of elements known as the Noble Gases that have been studied extensively over many years and are often used as models for pressure versus density curves because of their small interatomic interactions. Helium is also important with respect to the study of stars. Most stars are composed of mainly hydrogen and helium. Also, ^{4}He is known to become a superfluid at temperatures below 4.2 K. Thus, knowing the effects of pressure on a helium atom is necessary for a number of research fields.

4.2.1 Results and Discussion

In the following, helium is analyzed in a similar fashion as hydrogen, first by varying the hardness of the potential wall and then by varying the confining potential radius. For the changing of the stiffness parameter, n, from 2 to 102, similar trends to hydrogen were observed, namely a monotonic increase of the energies, shown in Figure 4.2.1. The confinement radius was set to $r_o = 1$ a.u. The hard-wall energy limit for this confinement is 1.06179 a.u. [29]. Again, the convergence was very slow to this limit, i.e. much higher values for n would be needed for convergence. Next, helium was squeezed from a confinement radius, r_o, of 10.0 a.u. down to a radius of 0.2 a.u. Like for hydrogen, the energy of helium rose as the radius of confinement was narrowed in Figure 4.2.2. In this plot, n remained at 30 and the energies go to the limit of -2.86 a.u., which is the total Hartree-Fock energy of a free helium atom [19].

Figure 4.2.3 shows the squeezing of helium by plotting wave functions of different confinement radii. These radii were then systematically decreased from 10.0 a.u. to 0.2 a.u. and plotted with the free atom wave function. This shows the gradual convergence of the confined atoms to the function of the free atom.

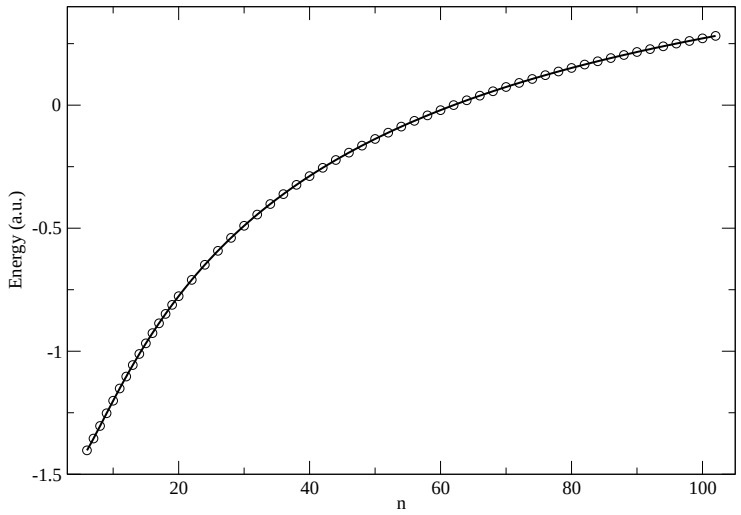

Figure 4.2.1: Energy values as the confinement wall is hardened and the radius is kept at $r_o = 1$ a.u.

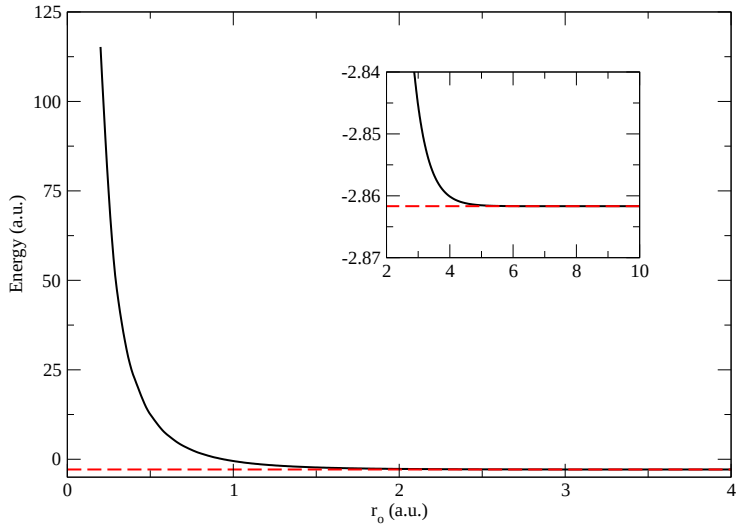

Figure 4.2.2: Energy values as the potential of the wall is kept at 30 and the radius of confinement, r_o, is varied up to 10 a.u. where it asymptotically approaches the Hartree-Fock energy for Helium, -2.86 a.u.

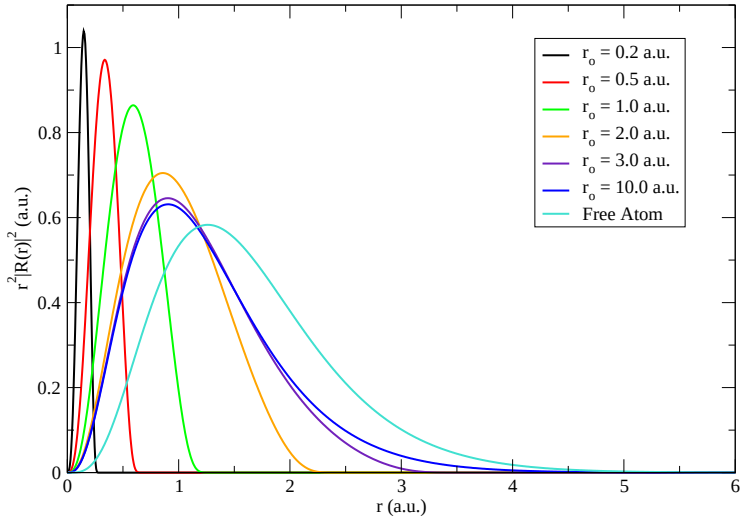

Figure 4.2.3: The probability density function of the radial distribution function, $P(r)$, at different r_o values.

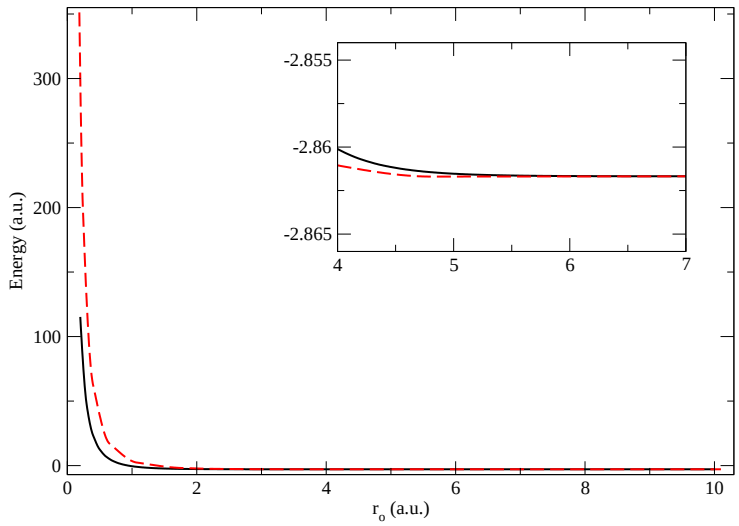

Figure 4.2.4: Energy values when integration was performed until r_o (dashed line) and the potential of the wall is kept at 30 and the radius of confinement, r_o, tends towards 10 a.u. (solid line).

Similar to the hydrogen atom analysis, the helium wave functions were next confined as the integration was performed only up to the confining radius, r_o. The resulting energies were then compared to the hard-wall data. The results are shown in Figure 4.2.4. For $r_o \geq 3$ a.u. the obtained energies approximated the hard-wall energy values well, while for smaller confinement radii the deviations are more noticeable. These wave functions with smaller confinement radii have a larger tails that extend past the limit of the confinement radii, r_o. Values of the confinement potential are the cause of this variation. The confinement potential that is used is not a hard wall. This makes the forcing of the wave function to zero at a certain point very difficult. Any fluctuation away from the hardwall potential results in a larger difference between the final energies depending on the amount that the tail extends over the limit.

The pressure versus volume plot, Figure 4.2.5, shows the values as they range from 6.915×10^2 Pa to 1.196×10^{16} Pa for pressure and $1.676 \times 10^{-32}\text{m}^3$ to $5.842 \times 10^{-28}\text{m}^3$ for the volume. Finally, the pressure versus density curve, in plot 4.2.6, shows a monotonic increasing trend. The pressures cover the same range as before, while the density ranges between 0.0137 and 396 $\frac{\text{g}}{\text{cm}^3}$.

For consistency, MCHF95 outputs of helium were compared with the helium calculations using the Gaussian03 program package. For $n > 2$, the program was not able to calculate the energy for a wide enough range of radii within Gaussian03. Therefore, $n = 2$ was used where analysis could be done on the full range from $r_o = 0.2$ to 10.0 a.u. When changing n and r_o (Figures 4.2.7 and 4.2.8 respectively), energies were found that asymptotically reached the proper aforementioned limits. For a very soft potential ($n = 2$) the Gaussian03 and the MCHF95 results are identical. For harder potentials (increasing n) convergence problems were encountered for Gaussian03 calculations starting already for $n \approx 8$.

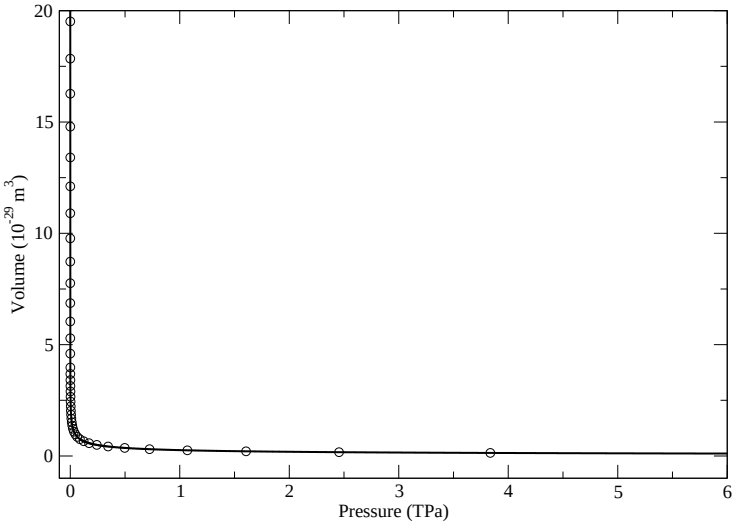

Figure 4.2.5: Pressure versus volume as the confinement radius, r_o, changes from 0.2 to 10.0 a.u. and the hardness, n, is 30.

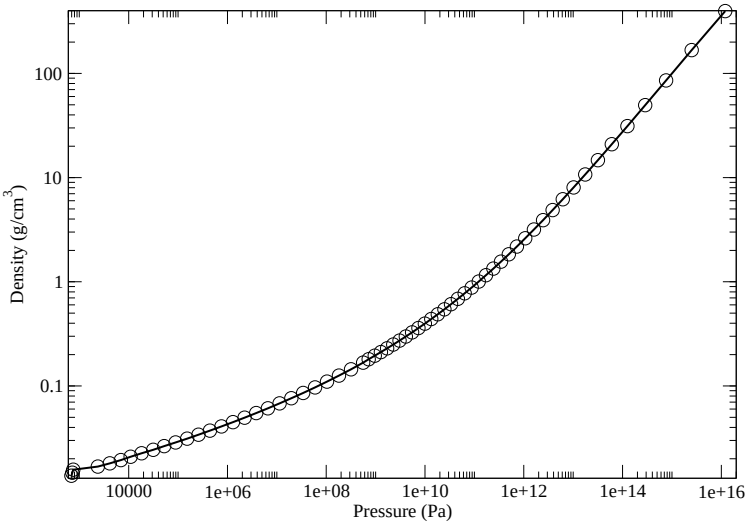

Figure 4.2.6: Pressure versus Density when $r_o/in[0.3, 10.0]$.

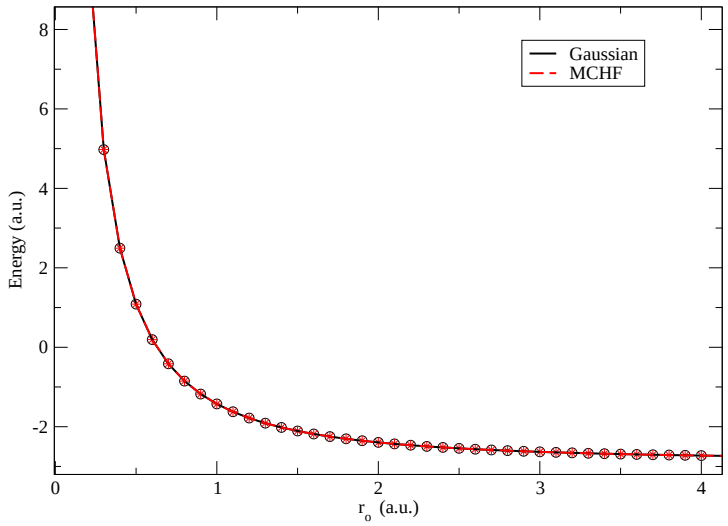

Figure 4.2.7: Energy calculated by Gaussian and MCHF, where $n = 2$ and $r_o \in [0.2, 4.0]$ a.u.

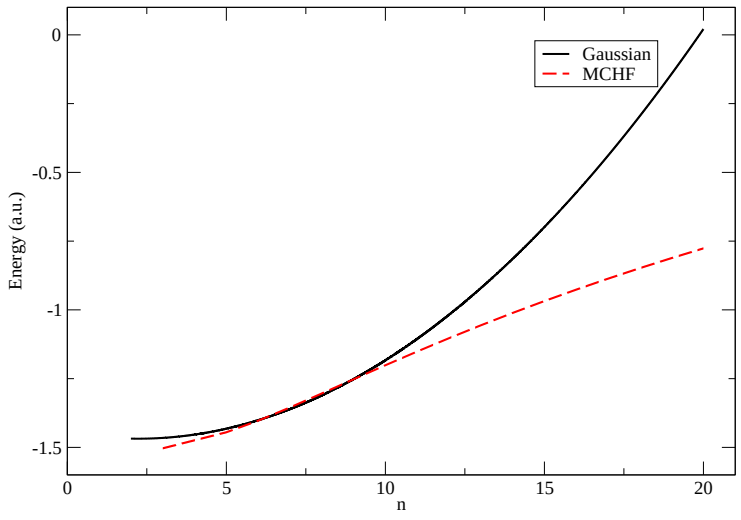

Figure 4.2.8: Helium: Energy calculated by Gaussian and MCHF, where $r_o = 1$ a.u and $n \in [0, 20]$.

4.3 Neon

Neon, like helium, is a Noble gas and is not solvable analytically. It will be easy to compare our calculated results with others since it is prevalent in a plethora of research topics. Neon is also found in older stars such as Red Giants and Super Giants which have begun to create rings of an evolved core that is slowly transitioning into solid iron. In his research of the planet Jupiter, Galileo discovered the existence of neon in the outer cloud layer of the gas giant. The presence of neon and helium are believed to be one of the contributing factors that keep the planet's inner temperature high.

4.3.1 Results and Discussion

The neon atom, with its 10 electrons, has a ground state occupation scheme of $1s^2 2s^2 2p^6$. For this reason, it required a larger minimum confining radius and larger basis sets. Each of these evoked many problems not seen with the other two elements.

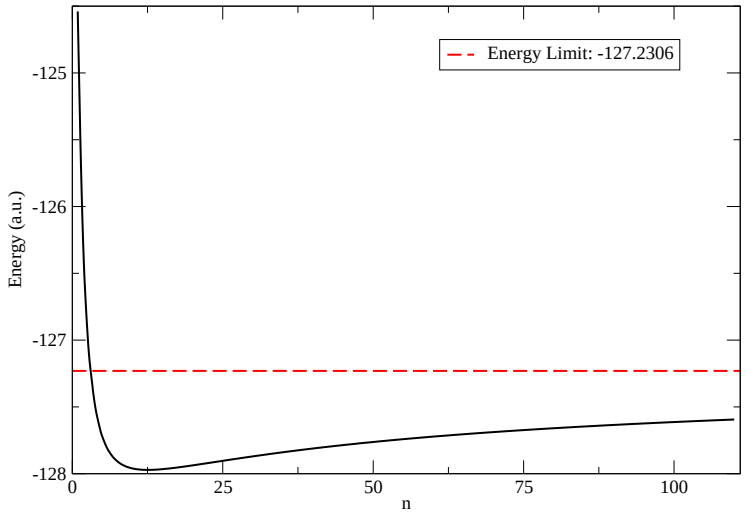

Figure 4.3.1: Energy values approached -127.2306 a.u., the ground state energy of neon in the hard-wall limit with a confinement radius of $r_o = 2$ a.u. This radius was used instead of $r_o = 1.0$ a.u. because the latter converged for only four integer stiffness values.

We began our studies of neon again with MCHF95 calculations of the ground state energy as n and r_o were varied. Figure 4.3.1 shows the succession of energy

values as $r_o = 2$ a.u. and $n \in [2, 110]$. The limit of this plot is -127.2306 a.u. [29] which is the hard-wall limit of the total Hartree-Fock energy of a Neon atom confined to 2 a.u. Figure 4.3.2 continues with the display of energy values as $n = 30$ and $r_o \in [1.3, 10.0]$ a.u. The limit of this plot is -128.5471 a.u. [19] which is the total energy of a free Neon atom. No energy values were obtained for $r_o \leq 1.3$ a.u. A probable explanation is that the rise in electron correlation makes convergence of the wave function more difficult. However, for $n = 0$ we can deduce that $\Sigma_{i=1}^{10} \left(\frac{r_i}{r_o}\right)^n \overrightarrow{1} 0$, when $n = 0$, thus we get the energy for $n = 0$ as -128.5471 + 10 a.u. = -118.5471 a.u.

To analyze the effects of the confinements in more detail, the probability density plots for each type of orbital were analyzed and compared to the density functions of the free atom orbitals. Figure 4.3.3 shows the $1s$ orbital. All probability density functions between 1.3 a.u. and the free atom, i.e. no confinement, are basically the same with minimal fluctuation. This is easily understandable due to the localization of its electron density close to the nucleus. The $2s$ and $2p$ orbital probability density plots are, however, influenced by the confinement from very small radii to the free atom as can be seen in Figures 4.3.4 and 4.3.5.

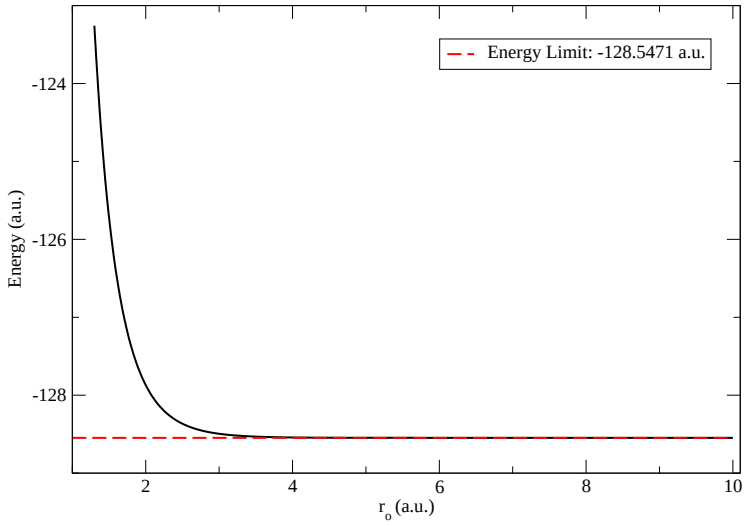

Figure 4.3.2: The energy values as the confinement radius is increased. As r_o tends towards 10 a.u., $n = 30$ and the energies approach the limit -128.5471 a.u., which is the energy of a free neon particle.

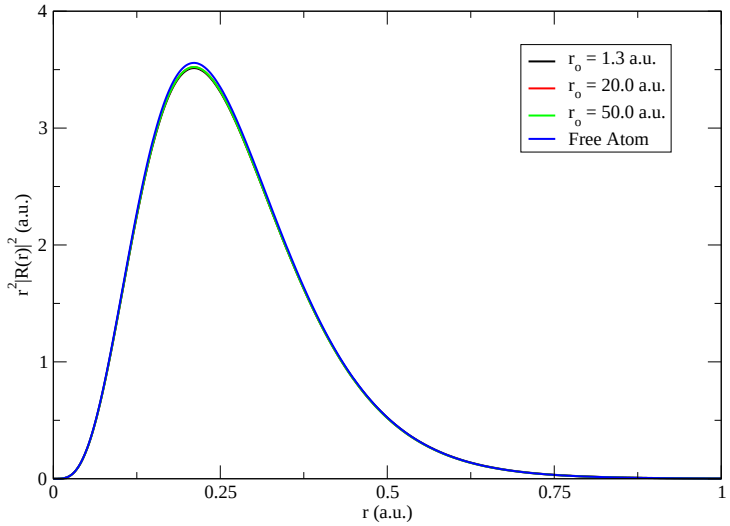

Figure 4.3.3: Probability density functions of the radial wave functions for the $1s$ orbital and $n = 1$.

In order to gain insight into the state of Jupiter's inner composition the pressure, and the densities were calculated for each energy value. These values were calculated as r_o varied between 1.3 and 10.0 a.u. Pressure declined from 1.46×10^13 Pa for $r_o = 1.4$ a.u. to 635 Pa, which was obtained for $r_o = 9.6$ a.u. The pressure inside Jupiter is projected to be between 3.5 and 4 TPa at the core. Thus, according to Figure 4.3.6, the radius of confinement is around 1.75 a.u. and the density is about 9.75 $\frac{\text{g}}{\text{cm}^3}$, which is not the average density of Jupiter, 1.33 $\frac{\text{g}}{\text{cm}^3}$ hence the core might not consist of neon.

In addition to looking at the pressure versus density curves, the pressure versus volume curve was also analyzed and displayed in Figure 4.3.7. The plot produced the expected trend: as volume decreases, pressure increases.

Finally, the energies were also calculated with the Gaussian03 software package and compared with the MCHF95 results (see Fig. 4.3.8 and 4.3.9). Again, difficulties in converging the results appeared for harder potentials and the program could not proceed beyond $n = 20$. From $n \approx 10$ one already denotes the onset of the convergence problems, most probably caused by insufficient basis sets. In contrast to MCHF, no

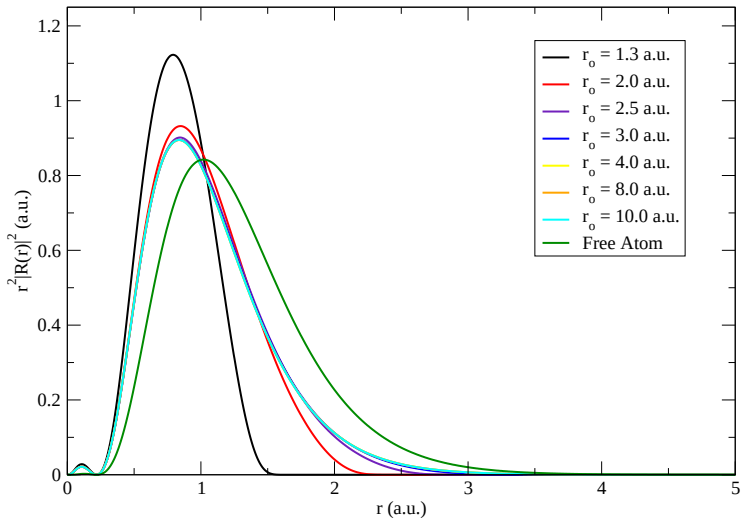

Figure 4.3.4: The probability density functions of the radial wave functions for the $2s$ orbital and $n = 1$.

problems were encountered as the confinement radius was decreased to 1 a.u.

In general both sets of Gaussian energies, for varying n and r_o, are in good agreement with the MCHF95 data when n is less than 10. Figure 4.3.8 shows the results as n was varied and $r_o = 2$ a.u. It shows a strange bend in the Gaussian03 values that proves even more that the basis set used was insufficient. The following figure, Figure 4.3.9, presents the energy values as n is set to 2 and the r_o values varied between 1.3 and 10 a.u. All energy values, up to $n = 10$ and $r_o = 10$ a.u., agreed very well and seem to approach the limit of the Hartree-Fock energy of a free neon atom, $E = -128.5471$ a.u.

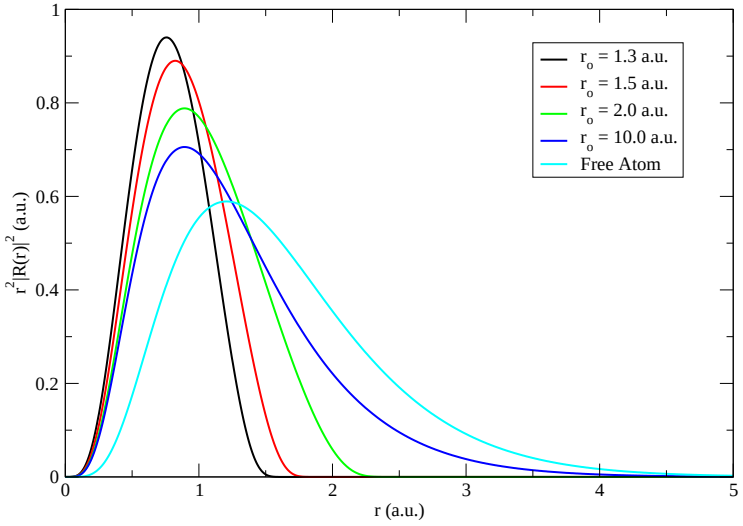

Figure 4.3.5: Probability Density Functions of the radial wave functions for the $2p$ orbital and $n = 1$.

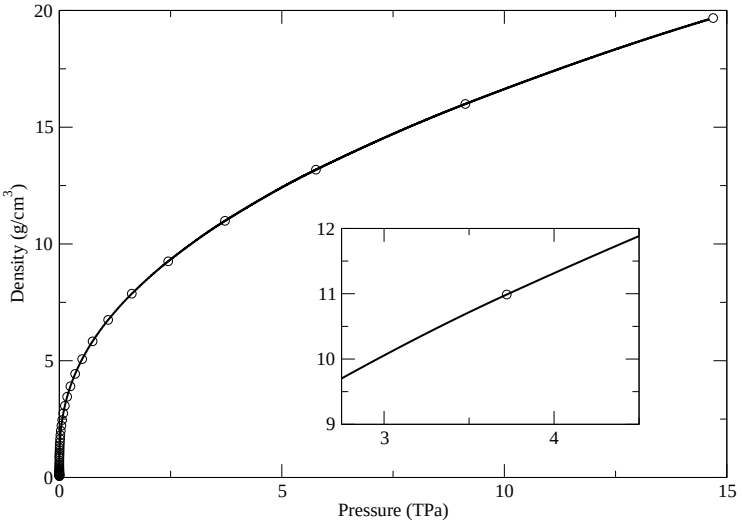

Figure 4.3.6: Pressure versus Density values while $n = 30$. The inset shows the hypothesized range of pressures for the interior of Jupiter.

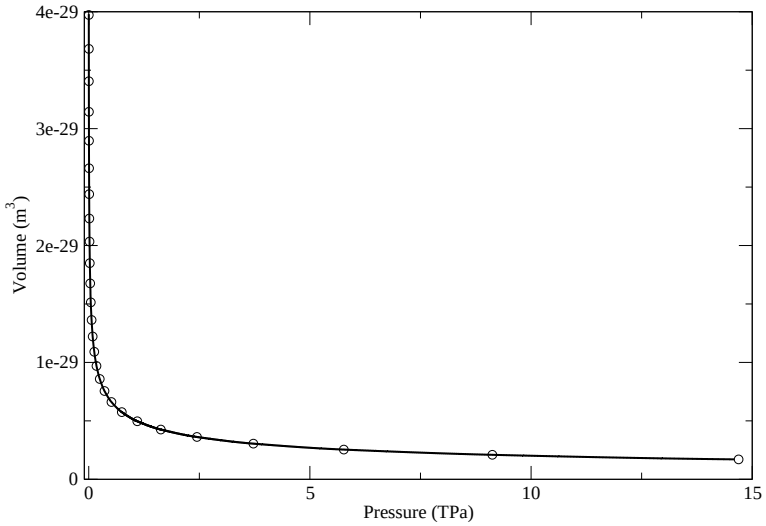

Figure 4.3.7: Pressure versus volume as r_o changes from 1.3 to 10.0 a.u and $n = 30$.

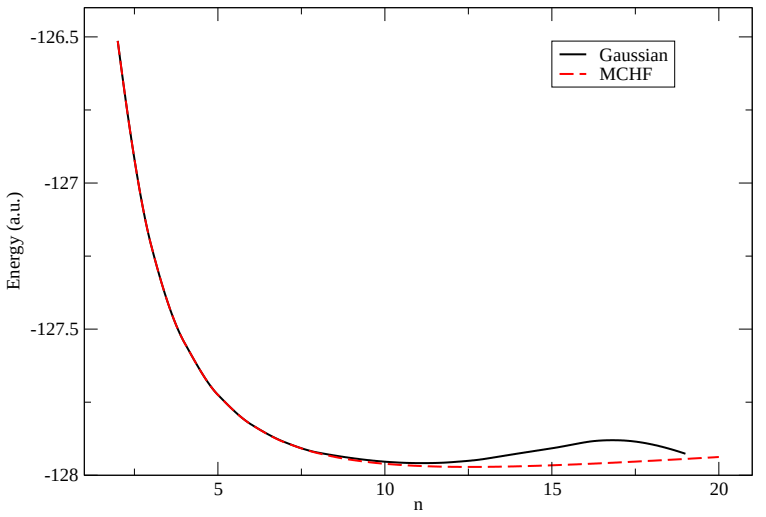

Figure 4.3.8: Energies calculated by the program package Gaussian03 and MCHF95, where $r_o = 2$ and n varies between 2 and 20.

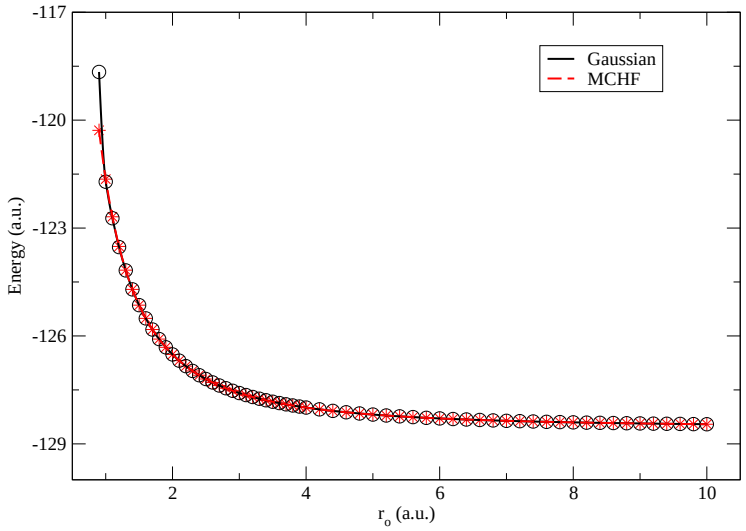

Figure 4.3.9: Energy values calculated by Gaussian and MCHF, where $n = 2$ and r_o increased from 1.3 to 10.0 a.u.

5 Conclusion and Future Goals

It is the stars,

The stars above us, govern our conditions...

William Shakespeare, 1564-1616, *King Lear*

This thesis investigated if the behavior of solids under extreme pressure can be modeled by confining a single atom in a spherical box. This confinement is easily implemented and can be used to calculate pressure and density values. Processing of the energies proceeded with out any problems for most combinations of confinement potential and radius. The only problems arose when the stiffness parameter of the confinement potential rose above 40, while r_o was kept at 1.0 or 2.0 a.u., and Neon was squeezed smaller than 1.3 a.u. which resulted in convergence issues and the incompleteness of sets of corresponding energies. In spite of the problems with the extreme situations, the calculations will be helpful in qualitatively describing the interiors of stars and planets by either proving or disproving current and future postulations.

The results from calculations using Gaussian03 basis sets agree quite well with the numerical results for weak confinement potentials, i.e. small n. For large n though, Gaussian basis set results often differ markedly or the calculations do not converge at all; this is due to the fact that different confinement situations would require different (optimized) basis sets to obtain results of comparable quality. This inherent deficiency of the basis set based methods prevents its future use for the investigation of confined atoms. In contrast to the basis set based calculations, the numerical calculations using MCHF95 are not biased by basis set deficiencies and converge for a wider range of r_o and n values. After full implementation of the confinement method in MCHF95, this method will open an efficient route to analyze more elements in a similar fashion.

Improving MCHF95, would include looking into the program and finding a way for MCHF95 to handle more extreme situations. Methods used, such as changing the grid or reading in the previous wave function, only improved the span of the results so

far. A grid needs to be implemented that will cluster most of the grid-points around the confinement radius, instead of the beginning of the graph, in order to be able to be as accurate as possible. The most dynamically changing areas need the most points and this is not necessarily at the beginning of the wave function as the logarithmic scale suggests. Moreover, for the initial guess of the wave function, the asymptotic limit of Kummer's differential equation, in the case for a confinement potential, needs to be explored. The question addressing whether Gaussian functions can be used for high pressure simulations, or not, needs to be investigated further. Our ultimate goal with neon, to calculate the range of values for $r_o = 1$ a.u. was unable to be attained even after extensive manipulation of the program.

A Appendix: Tables

I can find in my undergraduate classes,

bright students who do not know that the stars rise and set at night,

or even that the Sun is a star.

Carl Sagan, 1934-1996

n	E	n	E
1	5.7792135E-01	44.0	1.5585874E+00
2	5.9377128E-01	46.0	1.5780921E+00
3	6.1947291E-01	48.0	1.5965634E+00
4	6.5437492E-01	50.0	1.6140849E+00
5	6.9405265E-01	52.0	1.6307312E+00
6	7.3556048E-01	54.0	1.6465690E+00
7	7.7720643E-01	56.0	1.6616586E+00
8	8.1805785E-01	58.0	1.6760541E+00
9	8.5761939E-01	60.0	1.6898043E+00
10	8.9564685E-01	62.0	1.7029538E+00
11	9.3204106E-01	64.0	1.7155427E+00
12	9.6678666E-01	66.0	1.7276078E+00
13	9.9991619E-01	68.0	1.7391827E+00
14	1.0314888E+00	70.0	1.7502978E+00
15	1.0615774E+00	72.0	1.7609814E+00
16	1.0902609E+00	74.0	1.7712592E+00
17	1.1176197E+00	76.0	1.7811549E+00
18	1.1437327E+00	78.0	1.7906905E+00
19	1.1686758E+00	80.0	1.7998861E+00
20	1.1925210E+00	82.0	1.8087603E+00
22	1.2371848E+00	84.0	1.8173306E+00
24	1.2782148E+00	86.0	1.8256129E+00
26	1.3160357E+00	88.0	1.8336222E+00
28	1.3510130E+00	90.0	1.8413723E+00
30	1.3834616E+00	92.0	1.8488763E+00
32	1.4136527E+00	94.0	1.8561461E+00
34	1.4418206E+00	96.0	1.8631931E+00
36	1.4681686E+00	98.0	1.8700278E+00
38	1.4928738E+00	100.0	1.8766600E+00
40	1.5160909E+00	102.0	1.8830990E+00
42	1.5379556E+00		

Table 1: Hydrogen: Energies (in a.u.) of a squeezed hydrogen atom as a function of the stiffness,n, of the confinement potential when the confinement radius is fixed at $r_o = 1$ Bohr.

r_o	E	r_o	E
0.2	6.380538E+01	3.7	-4.831131E-01
0.3	2.774089E+01	3.8	-4.855127E-01
0.4	1.496764E+01	3.9	-4.875727E-01
0.5	9.058391E+00	4	-4.893415E-01
0.6	5.873278E+00	4.2	-4.921648E-01
0.7	3.977118E+00	4.4	-4.942466E-01
0.8	2.766624E+00	4.6	-4.957807E-01
0.9	1.952812E+00	4.8	-4.969102E-01
1	1.383462E+00	5	-4.977407E-01
1.1	9.723829E-01	5.2	-4.983505E-01
1.2	6.679070E-01	5.4	-4.987976E-01
1.3	4.375979E-01	5.6	-4.991248E-01
1.4	2.603021E-01	5.8	-4.993638E-01
1.5	1.217748E-01	6	-4.995382E-01
1.6	1.215816E-02	6.2	-4.996653E-01
1.7	-7.553218E-02	6.4	-4.997576E-01
1.8	-1.463471E-01	6.6	-4.998247E-01
1.9	-2.040055E-01	6.8	-4.998734E-01
2	-2.512896E-01	7	-4.999086E-01
2.1	-2.903104E-01	7.2	-4.999341E-01
2.2	-3.226904E-01	7.4	-4.999525E-01
2.3	-3.496904E-01	7.6	-4.999658E-01
2.4	-3.723009E-01	7.8	-4.999754E-01
2.5	-3.913067E-01	8	-4.999823E-01
2.6	-4.073355E-01	8.2	-4.999873E-01
2.7	-4.208930E-01	8.4	-4.999908E-01
2.8	-4.323894E-01	8.6	-4.999934E-01
2.9	-4.421596E-01	8.8	-4.999953E-01
3	-4.504790E-01	9	-4.999966E-01
3.1	-4.575748E-01	9.2	-4.999976E-01
3.2	-4.636357E-01	9.4	-4.999983E-01
3.3	-4.688188E-01	9.6	-4.999987E-01
3.4	-4.732559E-01	9.8	-4.999991E-01
3.5	-4.770575E-01	10	-4.999994E-01
3.6	-4.803170E-01		

Table 2: Hydrogen: Energies of a squeezed hydrogen atom when r_o was changed and the stiffness parameter, n, was fixed at 30.

r_o	E	Volume
0.2000	6.38121E+01	3.35103E-02
0.4000	1.49688E+01	2.68083E-01
0.6000	5.87369E+00	9.04779E-01
0.8000	2.76685E+00	2.14466E+00
0.8100	2.67085E+00	2.22609E+00
0.9100	1.88684E+00	3.15655E+00
1.0000	1.38359E+00	4.18879E+00
1.0100	1.33641E+00	4.31571E+00
1.0800	1.04488E+00	5.27667E+00
1.1500	8.09280E-01	6.37063E+00
1.4480	1.89720E-01	1.27173E+01
1.7110	-8.40200E-02	2.09816E+01
1.7780	-1.31980E-01	2.35442E+01
1.8000	-1.46300E-01	2.44290E+01
1.8350	-1.67810E-01	2.58819E+01
1.9020	-2.05010E-01	2.88217E+01
1.9343	-2.21230E-01	3.03152E+01
2.0000	-2.51250E-01	3.35103E+01
2.1782	-3.16090E-01	4.32894E+01
2.2000	-3.22650E-01	4.46022E+01
2.2005	-3.22800E-01	4.46327E+01
2.4720	-3.86280E-01	6.32753E+01
2.8070	-4.33080E-01	9.26437E+01
2.8130	-4.33730E-01	9.32390E+01
3.0000	-4.50450E-01	1.13097E+02
3.0413	-4.53550E-01	1.17833E+02
3.1920	-4.63170E-01	1.36231E+02
3.2130	-4.64340E-01	1.38938E+02
3.5287	-4.78030E-01	1.84049E+02
3.7520	-4.84390E-01	2.21247E+02
4.0000	-4.89310E-01	2.68083E+02
4.0062	-4.89430E-01	2.69331E+02
4.0680	-4.90370E-01	2.81989E+02
4.4153	-4.94370E-01	3.60553E+02
4.5765	-4.95600E-01	4.01503E+02
4.7916	-4.96850E-01	4.60819E+02
4.9336	-4.97480E-01	5.03014E+02
5.0000	-4.97730E-01	5.23599E+02
5.0200	-4.97800E-01	5.29907E+02
5.1157	-4.98090E-01	5.60795E+02
5.3706	-4.98710E-01	6.48869E+02
5.8010	-4.99350E-01	8.17706E+02
6.0000	-4.99520E-01	9.04779E+02
6.2253	-4.99660E-01	1.01058E+03
7.0000	-4.99880E-01	1.43676E+03
8.0000	-4.99960E-01	2.14466E+03
9.0000	-4.99980E-01	3.05363E+03
10.0000	-4.99980E-01	4.18879E+03

Table 3: Hydrogen: Energy values for ground-state hydrogen confined by a hard-wall when r_o was changed and $n = 30$. Calculated by Mathematica® .

References

[1] NASA and The Hubble Heritage Team. Supernova 1987A.

[2] K. Davis. American Association of Variable Star Observers: SN1987A Variable Star of the Month.

[3] T. C. Chan, K. S. Cheng, and et al. Could the Compact Remnant of SN1987A be a Quark Star? *The Astrophysical Journal*, 695(1):732–746.

[4] CICLOPS and NASA/JPL/Space Science Institute. PIA04866: Cassini Jupiter Portrait.

[5] P. J. Gierasch and P. D. Nicholson. *Jupiter*. World Book, Inc, 2004. `http://www.worldbookonline.com/wb/Article?id=ar293080`.

[6] R. E. Young. The Galileo probe: how it has changed our understanding of Jupiter. *New Astronomy Reviews*, 47:1–51, December 2003.

[7] D. Saumon and T. Guillot. Shock Compression of Deuterium and the Interiors of Jupiter and Saturn. *The Astrophysical Journal*, 609(2):1170–1180.

[8] L. T. Elkins-Tanton. *Jupiter and Saturn*. Chelsea House: an imprint of Infobase Publishing, 2006.

[9] C. Miller. Black Holes and Neutron Stars.

[10] K. M. Wong and R. Wenk. Crystals Reveal Earth's Hidden History.

[11] N. W. Ashcroft. Pressure for Change in Metals. *Nature*, 458:158–159, March 2009.

[12] R. J. Hemley and N. W. Ashcroft. The Revealing Role of Pressure in the Condensed Matter Sciences. *Physics Today*, pages 26–32, August 1998.

[13] H. K. Mao and P. M. Bell. Observations of Hydrogen at Room Temperature (25° C) and High Pressure (to 500 Kilobars). *Science*, 203:1004–1006, January 1979.

[14] Walter G. *Quantum Mechanics: An Introduction*. Springer, 1994.

[15] W. R. Johnson. *Atomic Structure Theory: Lectures on Atomic Physics*. Springer, 2007.

[16] This Mathematica® program was written by Christian Thierfelder in order to calculate the hard-wall pressures for hydrogen, 2009.

[17] H. Friedrich. *Theoretical Atomic Physics*. Springer, 1994.

[18] C. Froese-Fischer, 1991. This program uses the Multi-Configurational Hartree-Fock Method to calculate the energies of a single atom.

[19] C. Froese Fischer. *The Hartree-Fock Method for Atoms: A Numerical Approach*. A Wiley-Interscience Publication: John Wiley & Sons, 1977.

[20] J. M. Thijssen. *Computational physics*. Cambridge University Press, 2007.

[21] M. J. Frisch and et al. Gaussian 03, Revision C.02. Gaussian, Inc., Wallingford, CT, 2004.

[22] G. Kresse and J. Furthmüller. Efficient iterative schemes for *ab initio* total-energy calculations using a plane-wave basis set. *Phys. Rev. B*, 54:11169–11186, 1996.

[23] J. P. Perdew, K. Burke, and M. Ernzerhof. Generalized gradient expansion made simple. *Phys. Rev. Lett.*, 77:3865–3868, 1996.

[24] G. Kresse and D. Joubert. From ultrasoft pseudopotentials to the projector augmented-wave method. *Phys. Rev. B*, 59:1758–1775, 1999.

[25] P. E. Blöchl. Projector augmented-wave method. *Phys. Rev. B*, 50:17953–17979, 1994.

[26] E. V. Ludeña. SCF Calculations for Hydrogen in a Spherical Box. *The Journal of Chemical Physics*, 66(2):468–470, January 1977.

[27] B. J. Van Zeghbroeck. Principles of Semiconductor Devices: Bravais Lattices.

[28] *Encyclopedia of the Solar System*. Elsevier, 2007.

[29] E. V. Ludeña. SCF Hartree-Fock calculations of ground state wavefunctions of compressed atoms. *The Journal of Chemical Physics*, 69(4):1770–1775, August 1978.